












From Microwave Acoustic Filters to Millimeter-Wave Operation and New Applications

AMELIE HAGELAUER ^{1,2} (Senior Member, IEEE), **RICH RUBY** ³ (Fellow, IEEE),
SHOGO INOUE ⁴ (Member, IEEE), **VICTOR PLESSKY** ⁵ (Senior Member, IEEE),
KEN-YA HASHIMOTO⁶ (Life Fellow, IEEE), **RYO NAKAGAWA**⁷ (Member, IEEE),
JORDI VERDU ⁸ (Senior Member, IEEE), **PEDRO DE PACO** ⁸ (Senior Member, IEEE),
AMIR MORTAZAWI ⁹ (Fellow, IEEE), **GIANLUCA PIAZZA** ¹⁰ (Senior Member, IEEE),
ZACHARY SCHAFFER ¹⁰ (Student Member, IEEE), **ERNEST TING-TA YEN**¹¹ (Member, IEEE),
THOMAS FORSTER ¹² (Student Member, IEEE), **AND ANDREAS TAG** ¹² (Member, IEEE)

(Invited Paper)

¹Fraunhofer EMFT Research Institution for Microsystems and Solid State Technologies, 80686 Munich, Germany

²Technical University of Munich, 80333 Munich, Germany

³Broadcom, Inc., San Jose, CA 95131 USA

⁴Qorvo, Inc., Apopka, FL 32703 USA

⁵NanoRF Sàrl, 1015 Lausanne, Switzerland

⁶University of Electronic Science and Technology of China, Chengdu 610054, China

⁷Murata Manufacturing Co., Ltd., Nagaokakyo 617-8555, Japan

⁸Universitat Autònoma de Barcelona, 08193 Barcelona, Spain

⁹University of Michigan, Ann Arbor, MI 48109-1382 USA

¹⁰Carnegie Mellon University, Pittsburgh, PA 15213-3815 USA

¹¹Texas Instruments, Dallas, TX 75266-0199 USA

¹²Qorvo, 81829 Munich, Germany

CORRESPONDING AUTHOR: Amelie Hagelauer (e-mail: amelie.hagelauer@emft.fraunhofer.de).

The work of Chapter 5 was supported by the Research Project under Grant A1098531023601318. The work of Chapter 7 was supported by the Spanish Secretaría de Estado de Investigación, Desarrollo e Innovación under Grant PID2021-127203OB-I00. The work of Chapter 9 was supported in part by NSF under Award 2133388 and in part by DARPA under Award HR00112220026.

This work did not involve human subjects or animals in its research.

ABSTRACT This paper reviews the latest developments in microwave acoustic wave devices. After an introduction and brief history of bulk acoustic wave (BAW) and surface acoustic wave (SAW) devices, a review is given for guided SAWs and XBARS - two new technologies, which are promising for future 5G applications. Following this, we discuss recent simulation techniques, such as 3D finite element method (3D FEM) and simulation of nonlinearities, as well as filter synthesis. Next, a review on tunable and reconfigurable acoustics is given. Finally, we present the latest developments in microwave acoustics for millimeter-wave (mm-wave) operation as well as BAW oscillators.

INDEX TERMS Bulk acoustic wave (BAW) devices, filter, filter-synthesis, front-end, high power, MTT 70th Anniversary Special Issue, multiplexer, nonlinearity, resonator, surface acoustic wave (SAW) devices.

I. INTRODUCTION

For 30 years the success of microwave acoustics, mainly in mobile phones, has been unstoppable. So far, there is no end in sight to this success story. Microacoustic resonators have outperformed any other filtering technology for mobile phones because of their ability to attain very low losses in

a small form factor. In addition to new technologies, new areas of application in particular have evolved in recent years. In this paper we want to review the most important developments of the last years. Chapter 2 gives a short historical overview of Surface Acoustic Wave (SAW) and Bulk Acoustic Wave (BAW) technology and briefly introduces the latest

developments. Chapter 3 then gives detailed insight into the so-called guided SAW technology and how it can improve device Quality Factor Q , electromechanical coupling factor k^2 and Temperature Coefficient of Frequency (TCF) in particular. Subsequently, Chapter 4 deals with another new technology - the XBAR. This technology is particularly promising for the 3 to 7 GHz frequency range and can thus address current trends in the 5G technology. After an overview of these technologies, simulation techniques for resonators and synthesis methods for filters are discussed in Chapters 5–7. In recent years, FEM simulation, simulation of nonlinearities and filter synthesis have played a particularly important role. In Chapter 8, the achievements of the last years in the field of tunable and reconfigurable devices is presented. Extending the range of operation to mm-wave frequencies (up to 60 GHz) comes with fundamental questions related to the ability to operate at such high frequency with low loss, sufficient bandwidth and appropriate impedance levels. In Chapter 9 we briefly review the state-of-the-art in mm-wave acoustics and introduce a new class of resonators specifically designed to operate at these frequencies. In Chapter 10 we review the usage of microwave acoustics for oscillators.

II. HISTORY AND LATEST DEVELOPMENTS

In 1965 Professor White and his Graduate Student F. Voltmer published a memorandum for the Electronics Research Laboratories at UC Berkeley [1]. This memorandum outlined for the first time periodic Interdigital Transducers (IDTs) generating coherent sound waves in a piezoelectric film, when excited by an AC voltage. At that time, there were few applications of interest for this technology and both White and Voltmer moved on. However, the application space expanded well beyond anyone's imagination when wireless mobile phones were demonstrated by Motorola in 1973 [2].

The first DynaTAC cell phones used ceramic filters [3]. But the ceramic filters took up a significant amount of the phone board area. This created a huge opportunity for a new technology to help reduce the size of mobile phones. The newly discovered (re-discovered) piezoelectric devices quickly replaced ceramic filters.

A. SURFACE ACOUSTIC WAVE DEVICES

In 1992 Fujitsu Ltd. created filters using SAW resonators in a ladder topology (series and shunt resonator stages) [4]. Thus, the first compact filters using piezoelectrics were introduced into phones. Given the large and bulky size of the ceramic filters, piezoelectric filters offered low profile and good insertion loss. Ladder stage resonator series/shunt pairs made up of a thin metal layer could be photo-lithographically patterned and then etched onto a piezoelectric substrate.

As demand for cell phones grew and the interface technology (starting with AMPS then GSM and later CDMA protocols¹) became more complex, SAW filters matched the

demand by dramatically improving performance and flexibility. GSM and CDMA bands covered multiple frequencies at and below 1 GHz. And here, SAW ruled supreme, specifically LTSAW devices using a Lithium Tantalate (LiTaO_3 , LT) substrate. However, the relatively low barrier of this technology created a lot of competition and commoditization (i.e. low prices). SAWs using LT, and especially Lithium Niobate (LiNbO_3 , LN) piezoelectrics has issues with the TCF. The TCF for LN was so high that the industry pivoted towards LT devices. But even LTSAWs high channel TCF was ≈ -50 to -60 ppm/C. This excluded SAW filters from the more demanding duplexer applications like Band B2, where the guard band between Tx and Rx was $\approx 1\%$.

In early 2004, Murata introduced the Temperature Compensated SAW (TCSAW) [5]. This allowed SAW technology to deploy 2 GHz technology. Band 1 was particularly suited for TCSAW. Many of the top SAW Filter technology companies followed suit by introducing their own technical versions of TCSAWs [6] or simply copying Murata's innovation.

Technology innovation seemed to have stalled at this point in time (around 2004/2005), and no new invention appeared to exist for SAW devices besides advantages in packaging technologies [7]. Although TCSAWs were technically much more challenging to make than traditional LTSAWs, intense commoditization of TCSAW technology still occurred in the following decade.

Both LTSAWs and TCSAW filters suffer from poor power handling at higher frequencies (much above 1 GHz). The problem is that power density increases by f^3 for all piezoelectric resonators. By 2 GHz, the quality and robustness of TCSAW and LTSAW filters was found wanting. This was the 'state of the art' for SAW technology from 2004 till 2016. By 2010 or later, approximately billions of SAW filters were sold into the cell phone market every year. But, in 2016, a new kind of SAW filter (called "Incredibly High Performance" or IHP) was introduced – again by Murata [8].

The key breakthrough technology was to thin the piezo layer down to less than $1\ \mu\text{m}$. This was accomplished by bonding a piezo wafer to a silicon wafer using a thin oxide interface and then 'thinning' down the piezo (typically LT). The underlying Si and SiO_2 greatly reduced the TCF and the LT/ SiO_2 interface 'trapped' the electric fields inside thin LT that both enhanced k^2 and more important, greatly improved Q . Due to the better heat extraction created by the Si substrate, power handling of these IHP SAW devices was inherently better than conventional SAW devices.

B. BULK ACOUSTIC WAVE DEVICES

Starting in 1980 [9], [10] a different piezoelectric technology - Bulk Acoustic Wave (BAW) – was introduced.² The geometry of BAW filters, being a 'bulk' device, lent itself to handling high powers at high frequencies relative to SAW devices. Early papers focused on ZnO as the piezoelectric layer. For many reasons, this was a bad choice. However, until

¹Mobile Phone standards and protocols: Advanced Mobile Phone Service (AMPS), Global System for Mobile Communications (GSM) and Code Division Multiple Access (CDMA)

²Within BAW technology, a distinction is made between Thin Film Bulk Acoustic Resonators (FBAR) and Solidly Mounted Resonators (SMR).

1980, there was no other viable choice for the piezoelectric material. But, in 1981 Ken Lakin published a key paper on the ability to deposit AlN using sputtering techniques [11]. The discovery that random AlN dimers ‘showing’ down on a substrate would somehow align themselves into a highly textured *c*-axes film was quite amazing. Unfortunately, very few researchers appreciated this fact and Ken Lakin who left his Professorship to start up his company TFR (later on incorporated into Triquint and nowadays part of Qorvo, Inc.) was pretty much an outlier in the field. In 1980 he laid out a vision showing that the small size and potential performance of a Thin Film Resonator device had great potential [12]. Few people listened and few papers were published between 1980 and mid 1990’s due to the intrinsic challenges (some would say insurmountable challenges) facing BAW – not the least being the relatively low technical barrier for SAW devices a mature filter technology. But as the burgeoning demand and popularity of cell phones took hold, the need for better and smaller filters drove more companies and researchers to re-evaluate BAW technology. This was partially documented in Chapter 5 of K. Hashimoto’s book, Bulk Acoustic Wave Filters for Communications [13]. This chapter also covers the breakthroughs on perimeter design of BAW resonators. This innovation comes from the realization that most of the losses in a free standing membrane comes from anchor point losses. Stop the energy loss here and the Q jumps up by large amounts (more than 2 times).

By 2009, BAW filters, duplexers and multiplexers dominated nearly all high end mobile devices. Demand for high performance filters with good RF properties and power handling at high frequencies grew at a phenomenal rate. The manufacturing challenge, however, kept many competitors out of the field. By 2009/2010, the technology for BAW had reached its pinnacle with Q ’s on the order of 4,000 and proven ruggedness. Around this time, an obscure research paper from Akiyama et al. [14] showed that the coupling coefficient could be made higher than the intrinsic coupling coefficient of pure AlN. As it turns out, for many filter applications, larger coupling coefficient has much greater value for filter design than higher Q . By 2016, BAW filters, duplexers and multiplexers containing Scandium (Sc) doped AlN were on the market. Today, it is estimated that over 10 billion filters in mobile devices use ScAlN BAWs. Another trend observed for BAW is the extension of the technology to ever higher frequencies. The original breakthrough for BAW commercialization was achieved for the challenging B2 mentioned before for which the SAW technology was not good enough at that time. B2 is sitting just below 2 GHz. However, since then the frequency supported by BAW technologies continued to increase in the same manner as new bands were introduced for LTE and 5G. Nowadays, BAW technology has been commercialized for the frequency range from 1 GHz to above 8 GHz [15]. Fig. 1 shows simulation and measurement results for a BAW filter designed for UWB-Ch9 operating around 8 GHz.

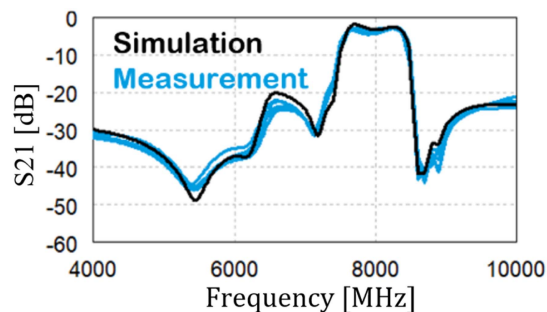


FIGURE 1. BAW filter for UWB-Ch9.

III. GUIDED SAW

As mentioned before, one of the most significant breakthroughs in SAW technology in the last 5 years is a drastic performance enhancement in resonator Q as well as k^2 and TCF for shear horizontal (SH) SAW devices by using a thin piezoelectric layer such as LT or LN bonded on a support substrate. The LT/LN thickness is less than the SAW wavelength and typically in the submicron range. This technology was enabled thanks to great advances in fabrication techniques of bonded wafers with a precisely controlled thin film piezoelectric layer which is not a deposited film but made from a single crystal wafer by means of mechanical polishing or smart cut [16]. As already mentioned Murata proposed configurations using Si as a support substrate (LT/SiO₂/AlN/Si and LT/SiO₂/Si), demonstrated spectacular performances ($Q = 4,000$ at 2 GHz, TCF = -8 ppm/K) [8], [17] and commercialized duplexers and multiplexers. Later, other configurations using different support substrates such as quartz [18], [19], [20], sapphire [20] and SiC [21] were proposed and demonstrated. In the literature, piezo on insulator (POI), guided SAW, layered SAW, thin film SAW or hetero acoustic layer (HAL) SAW are alternate denominations for IHP SAW technology. In this section, the name “guided SAW” is chosen and the mechanisms of how the guided SAW technology improves Q , k^2 and TCF are briefly reviewed [22].

A. IMPROVEMENT OF QUALITY FACTOR

LT in 42° YX cut (42Y LT) is a widely used SH SAW substrate and its orientation is chosen to minimize the BAW radiation loss (leaky loss) [23]. However, even 42Y LT cannot fully suppress the BAW radiation. The remaining BAW radiation, which mainly consists of slow shear wave / shear vertical (SV) wave displacements, is thought to be a dominant loss mechanism for 42Y LT SAW. Fig. 2(a) shows the simulated admittance and conductance for the conventional 42Y LT SAW using a 2D periodic FEM/BEM model [24]. The model has 10% λ thick aluminum electrodes (λ : 2 times the electrode period) and no material losses in 42Y LT or aluminum which means that the calculated loss is only due to a radiation of the acoustic energy into the substrate. The finite conductance which is observed in the simulation result near

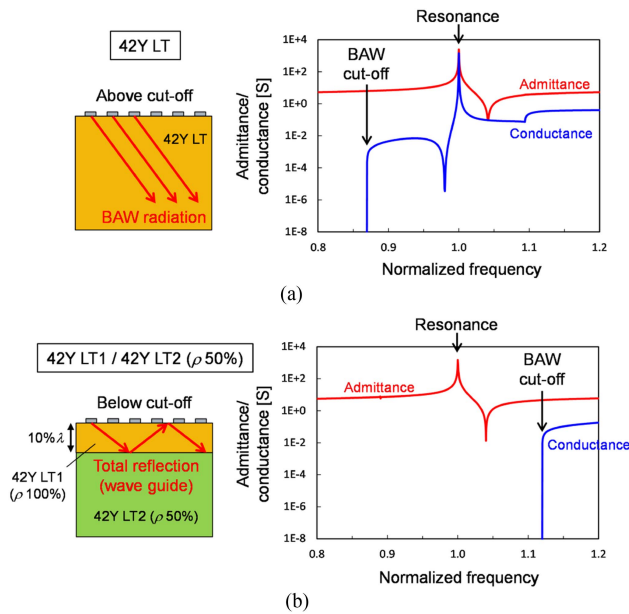


FIGURE 2. FEM/BEM simulation results for (a) conventional 42Y LT SAW and (b) guided SAW [22].

the resonance/anti-resonance frequency indicates that there is an acoustic leakage loss due to the BAW radiation into the substrate. Therefore, the Q for 42Y LT SAW is not very high in general.

The guided SAW structure with a thin LT layer bonded on a support substrate shown in Fig. 2(b) improves Q by confining the BAW radiation into the thin LT layer. The slow shear bulk wave as well as fast shear bulk wave are totally reflected at the bonding interface due to the faster velocity of the support substrate and guided into the thin LT layer as illustrated in Fig. 2(b). This is a similar principle to an optical waveguide, leading therefore to the chosen denomination of “guided SAW.” The guided SAW model shown in Fig. 2(b) was simulated with FEM/BEM. The model used a virtual support substrate material (42Y LT2) that has the same constants as a regular 42Y LT1 except for the mass density ρ . ρ for LT2 was reduced to 50% of ρ for LT1 to increase the velocity in LT2. The thickness of LT1 and aluminum electrodes were set to $10\% \lambda$. Fig. 2(b) shows the simulated admittance and conductance for the guided SAW model of thin LT1 on LT2. The conductance near the main SAW response is zero which means that there is no acoustic leakage loss due to the BAW radiation and the acoustic energy is well guided. Therefore, a high Q can be achieved with a structure having a piezoelectric layer bonded on top of a faster substrate.

The total elastic displacement distributions in the substrates for the conventional 42Y LT SAW and the guided SAW (42Y LT1/42Y LT2) were calculated using FEM to visualize the suppression of BAW radiation and are shown in Fig. 3(a) and (b), respectively. For both models, the same resonator, with 80 transducer electrodes, 40 reflector electrodes on each side of the transducer, $10\% \lambda$ thick aluminum electrodes and

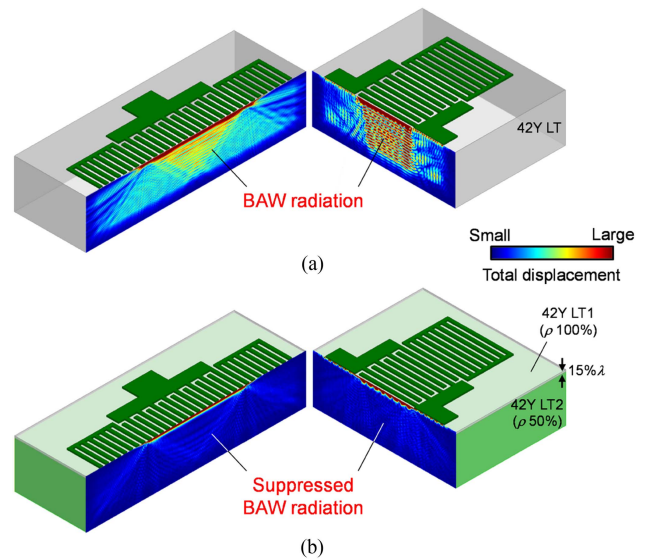


FIGURE 3. Simulated total displacement distributions in substrates by FEM for (a) conventional 42Y LT SAW and (b) guided SAW [22].

20λ wide aperture, is simulated. In Fig. 3(a), the substrate thickness of 42Y LT is 20λ . In Fig. 3(b), the thicknesses of 42Y LT1 and LT2 are $15\% \lambda$ and 20λ , respectively. 42Y LT2 has 50% of ρ for 42Y LT1 and the remaining constants for 42Y LT2 are the same as those for 42Y LT1. Fig. 3(a) and (b) display the same range of the displacement with the same color scale. Fig. 3(a) exhibits that a large amount of acoustic energy leaks into the substrate which is the dominant loss mechanism for conventional 42Y LT SAW. While Fig. 3(b) confirms that BAW radiation is significantly suppressed with the guided SAW structure and a much higher Q is expected.

B. IMPROVEMENT OF ELECTROMECHANICAL COUPLING FACTOR

One main reason why the guided SAW has a larger k^2 may be that the transducer on the guided SAW substrate normally has a smaller capacitance compared to that of the bulk LT/LN substrate because the support substrate tends to have a lower dielectric constant than LT/LN. Furthermore, LT/LN is thin enough for the electric field from the transducer to reach the support substrate. If the transducer capacitance is reduced without impacting the transduction efficiency, k^2 increases. Another reason for the larger k^2 of the guided SAW may be that the total stiffness of the guided SAW substrate may be softer than that of the bulk LT/LN substrate. For example, most elastic constants for silicon or quartz are smaller than those for LT/LN that makes the total stiffness of the bonded wafer softer. If the stiffness of the substrate is softer, k^2 increases. Fig. 4 shows the simulation results of k^2 for IHP SAW (LT/SiO₂/AlN/Si) as a function of the LT and SiO₂ thicknesses [17]. k^2 increases with reducing the LT thickness due to smaller transducer capacitance, but when LT is too thin ($< 0.15\lambda$), k^2 decreases possibly because of the less efficient

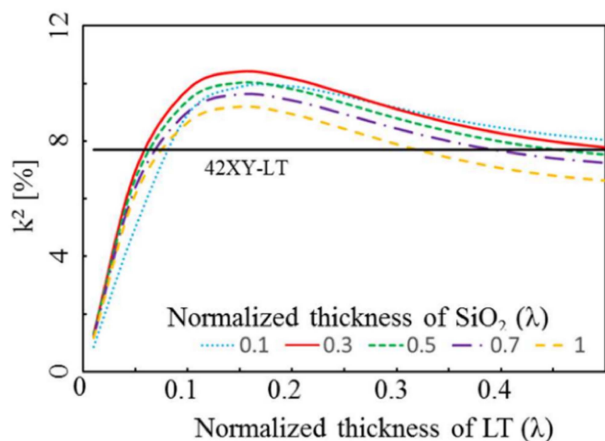


FIGURE 4. Simulated k^2 vs. LT and SiO_2 thicknesses for LT/ SiO_2 /AlN/Si configuration [17].

transduction. k^2 also increases with the SiO_2 layer due to further smaller transducer capacitance and less stiffness. However, when SiO_2 thickness is thicker than 0.3λ , k^2 decreases. This may be because more acoustic energy is in SiO_2 and less energy is in LT. Therefore, it is important to optimize the substrate stack to maximize k^2 .

C. IMPROVEMENT OF TCF

A better TCF can also be achieved with the guided SAW structure. TCF is a linear combination of temperature coefficient of velocity (TCV) and coefficient of thermal expansion (CTE), i.e., $\text{TCF} = \text{TCV} - \text{CTE}$. With the guided SAW structure, potentially both TCV and CTE would improve. With the bonded wafer configuration, the thermal expansion for the piezoelectric layer is constrained by the support substrate which normally has a smaller CTE than the piezoelectric layer, and the effective CTE of the piezoelectric layer becomes close to the CTE of the support substrate. When the piezoelectric layer thickness is very thin, a certain amount of acoustic energy propagates as an evanescent wave in the support substrate, which normally has a better TCV than the piezoelectric layer. Therefore, the TCV of the whole structure improves. If a SiO_2 layer is inserted below the piezoelectric layer like in IHP SAW, the positive TCV of SiO_2 also helps to improve the total TCV. As such, the guided SAW structure improves both CTE and TCV, resulting in better TCF.

D. PERFORMANCE EXAMPLES OF GUIDED SAW

Fig. 5 shows examples of measured performances (admittance and Bode Q_{Bode}) of guided SAW one port resonators working at 1 GHz [20], [22]. As a reference, results for a conventional 42Y LT SAW resonator are also shown in black. Aluminum electrodes are used for all cases. The red curves are for a 42Y LT ($30\%\lambda$)/sapphire stack and the blue curves are for a 42Y LT ($15\%\lambda$)/Z-prop. quartz stack. The k^2 for the LT/sapphire and LT/quartz are 9.0% and 9.9%, respectively, while the conventional LT SAW has an 8.0% k^2 . Max. Q for LT/sapphire

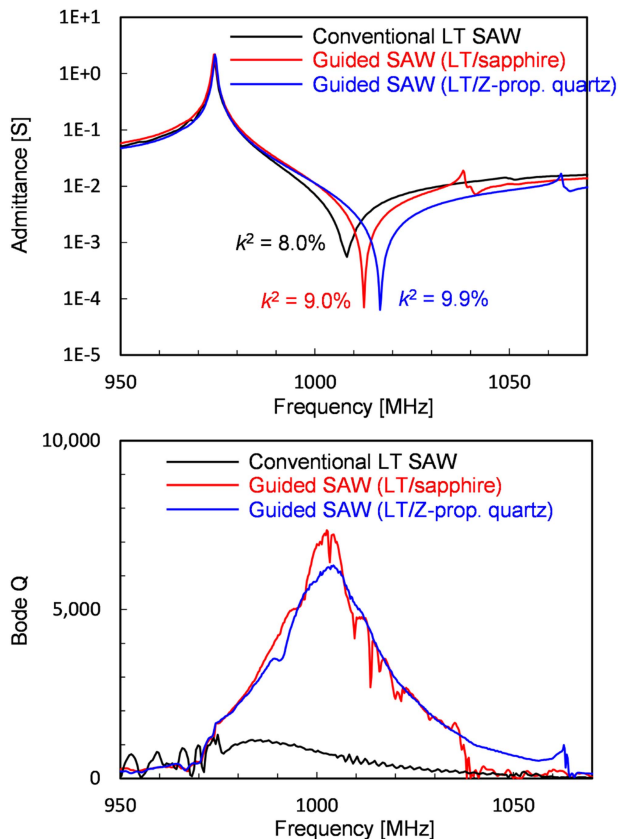


FIGURE 5. Measured admittance and Bode Q_{Bode} of LT/sapphire and LT/Z-prop. quartz guided SAW [20], [22].

and LT/quartz are higher than 7,000 and 6,000, respectively, which are about 7 and 6 times higher than the conventional LT SAW. TCF for the conventional LT SAW, LT/sapphire and LT/quartz are -38 ppm/K, -2 ppm/K and -23 ppm/K, respectively. As such, the guided SAW is a very promising technology with high Q , large k^2 and good TCF.

IV. XBAR

For current and future 5G mobile phones there is a need for filters in the 3 GHz to 7 GHz frequency range. They require similar filter characteristics as those used in the 2 GHz range: small, low cost, with low loss and excellent performance. So far only BAW technology has been able to meet those requirements as reviewed in section II.B. while LTSAW, TCSAW and IHP SAW have essential difficulties to meet these requirements. Recently, another technology - the laterally excited bulk acoustic wave resonator (XBAR) [25], [26] - has been invented and has shown promise to meet these specifications.

The device is based on a submicron-thin mono-crystalline layer (membrane) of LN suspended over a cavity in Si substrate. Such wafers with thin LN on Insulator are now commercially available [27] due to recently developed crystal ion-slicing technology.

The idea of exploiting the Lamb mode A1 which can have high phase velocity and strong coupling in a LN membrane

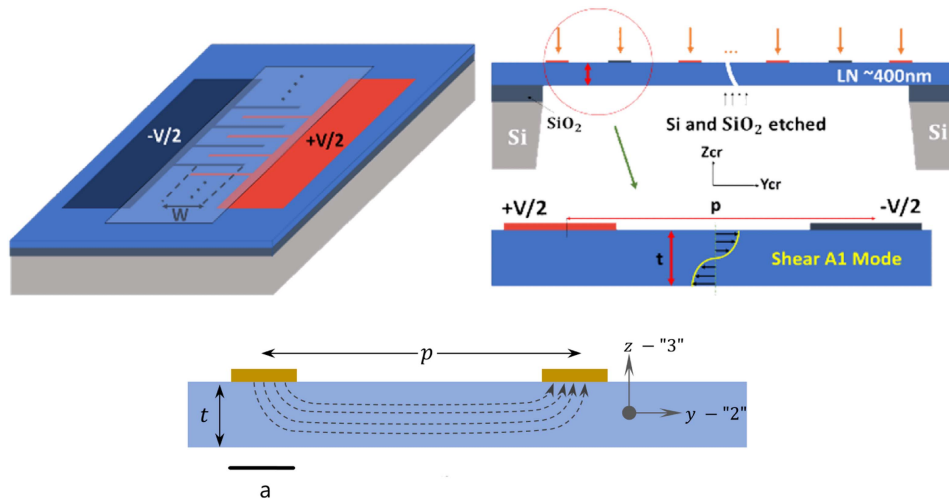


FIGURE 6. XBAR geometry [25], [26], [31], schematically - proportions are not observed.

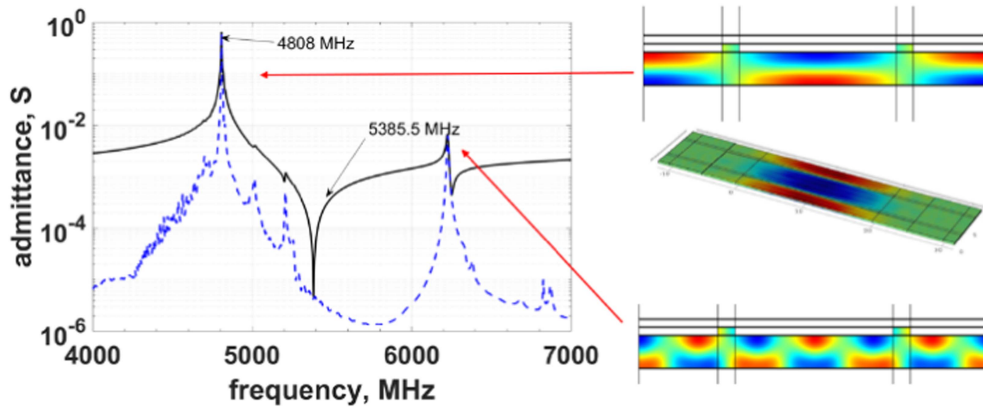


FIGURE 7. FEM-simulated XBAR performance; black solid line is for $\text{abs}(\text{Adm})$, dotted line – $\text{real}(\text{Adm})$ [26].

with a specifically chosen cut was proposed in the pioneering paper by M. Kadota [28]. Now, with ion-sliced LN layers of different cuts which can be transferred on different substrate there is the possibility to develop such devices that are potentially suitable for mass-production.

A resonator (XBAR) to be used in ladder-type filters for mobile phones, must satisfy a few criteria: a) the impedance at the resonance must be small, e.g. 1Ω and at the anti-resonance must be high, e.g. $1,000\Omega$, b) the Resonance-anti-Resonance (R-a-R) relative frequency gap must be around relative filter passband, c) Q at resonance frequency must be sufficiently high, and d) static capacitance C must correspond to 50Ω ($1/\omega C \approx 50\Omega$).

In this section it is shown that XBARs can have these demanded features. In Section IV-B a new version of the laterally excited resonator, a type of inverted XBAR with the crystalline membrane attached by electrodes to a substrate with high acoustic velocity, is presented.

A. XBAR: IDEA AND PROPERTIES

Fig. 6 shows the basic geometry of an XBAR. The key features are:

- The LN membrane with sub-micron thickness t is suspended over a cavity in the substrate and is attached by all sides to the substrate
- The transducer electrodes with alternating polarity, as in IDT for SAW, are situated at the distance $p \gg t$, and their width $a \ll p$, Fig. 6.

The horizontal electric field created by the electrodes inside the LN membrane, see Fig. 6, generates stresses due to the piezoelectric effect. If the cut is selected with strong piezo-modulus e_{15} (it can be, e.g., ZY-LN or 128° LN) the fundamental mode shear wave resonance with membrane thickness equal to half of wavelength can be excited between the electrodes. Fig. 7 shows the admittance curve of an XBAR and acoustic field distribution in this device. The standing wave with $\lambda/2 = t$ is excited between electrodes

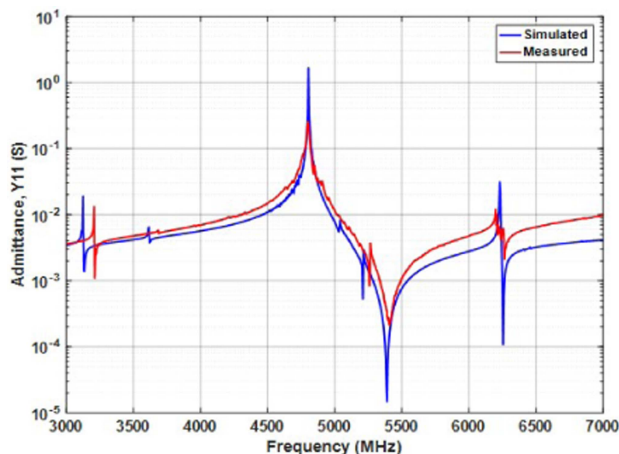


FIGURE 8. Measured XBAR performance versus FEM simulation. Small number of electrodes $N_t = 50$. For details see [29].

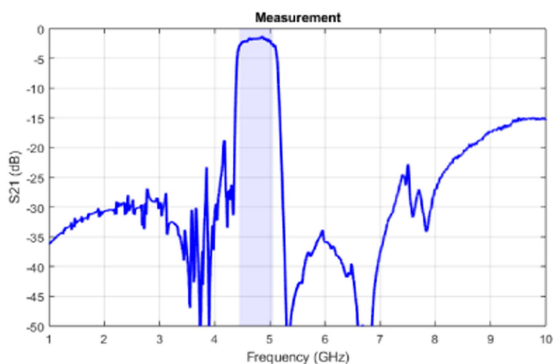


FIGURE 9. Measured XBAR filter performance, see [32].

with zero amplitude under the electrodes. This distribution of amplitudes is close to A1 anti-symmetric Lamb mode [28].

First XBARs were manufactured in NEMS Laboratory of Prof. L. G. Villanueva [26]. Dependencies of the resonator admittance on the device geometry, parasitic responses, Q , etc. were studied experimentally [29], [30]. Fig. 8 shows one of such measured curves.

The low loss level in XBAR technology is due to the small role played by electrodes – they only create the electric fields, but almost do not participate in the acoustics. Material acoustic losses in LN correspond to $Q > 5,000$ at 5 GHz. However, many other loss mechanisms are present, especially resistive losses, excitation of parasitic modes, acoustic losses and resonances in thick electrodes, leakage of energy in the aperture direction, etc.

One can see that XBARs satisfy the above formulated criteria for being used in “ladder” filters: three and more orders of resonance ($\approx 1\Omega$) to anti-resonance ($\approx 1,000\Omega$) impedance ratio with a large relative R-a-R gap of 10% and more, corresponding to n79 5G filter specification.

The first ladder filters have shown excellent performance [32] with around 1 dB min. insertion loss (IL) (Fig. 9). Now the laboratory samples of XBARs have less than 1 dB

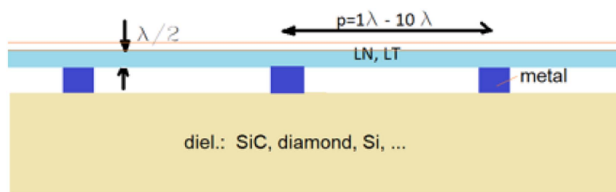


FIGURE 10. New laterally excited resonator [34] with the LN membrane supported on a substrate by pedestals (electrodes of the transducer).

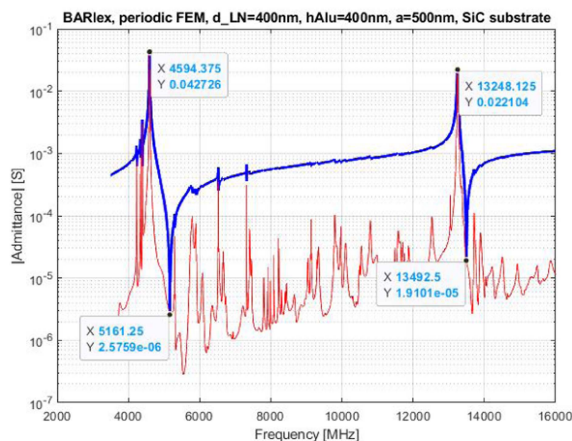


FIGURE 11. Simulated “inverted XBAR” performance [34].

IL [32], [33] and satisfy many 5G mobile phone specifications.

Ignoring the parasitic modes, the admittance of an XBAR can be described by a simple formula [31], with tunable frequency, coupling, static capacitance, etc., - similar to coupling of modes (COM) model used in SAW device design.

There are still the remaining XBAR challenges to solve for commercialization, e.g.: increase of power handling, trimming of frequency, mechanical robustness of the device.

B. INVERTED XBAR

As an attempt to solve these problems in [34] an inverted XBAR design with a LN membrane supported by the electrodes attached to a substrate with high acoustic velocity (Fig. 10) is proposed. The electrodes of the transducer play here the role of pedestals making the device structure more robust. Moreover, the power-handling in this resonator will be radically improved because the heat generated mainly in the electrodes is evacuated directly to the substrate through the large bottom area of the electrodes. The FEM simulations show parameters of the admittance curve comparable with standard XBAR (see Fig. 11).

V. ADVANCED FEM SIMULATION

Accurate and fast simulation tools are always demanded for the development of high-performance SAW and BAW devices [35]. The finite element method (FEM) has been widely

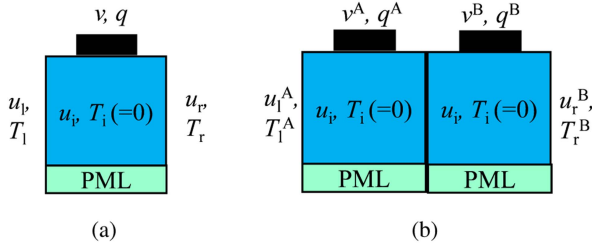


FIGURE 12. Unit cell of SAW resonator [41].

used for the purpose owing to its versatility [36]. In this section, advanced FEM simulation for BAW and SAW devices are reviewed. Previously its applicability was limited to small size problems because of required computer resources, but recent rapid advancement of computer technologies enables it to be applied to extremely large size problems. Therefore, full three-dimensional (3D) FEM has been applied to simulate whole BAW resonators [37]. On the other hand, for SAW resonators, its application was limited to parameter derivation for behavior models such as the COM theory [38] because of the large model size. In 2016, Koskela, et al., proposed the hierarchical cascading technique (HCT) for acceleration of two-dimensional (2D) FEM analysis of SAW devices [39], [40], [41]. In HCT, the simulation model is decomposed into small unit cells such as shown in Fig. 12(a) representing one grating period. In Fig. 12(a), PML is the perfect matching layer [42] placed to avoid wave reflection at the back surface. The FEM matrix of each unit cell is written as

$$\begin{pmatrix} A_{11} & A_{12} & 0 & A_{14} \\ A_{21} & A_{22} & A_{23} & A_{24} \\ 0 & A_{32} & A_{33} & A_{34} \\ A_{41} & A_{42} & A_{34} & A_{44} \end{pmatrix} \begin{pmatrix} u_l \\ u_i \\ u_r \\ v \end{pmatrix} = \begin{pmatrix} T_l \\ 0 \\ T_r \\ -q \end{pmatrix} \quad (1)$$

where A_{ij} are sub-matrices, and u , T , v and q are displacements (DOFs), stress, and electric potential and charge on the electrode, respectively. Subscripts l , r , and i indicate values at left boundary (l), the right boundary (r), and interior (i), respectively, of the unit cell. Elimination of u_i reduces (1) to the following B -matrix form:

$$\begin{pmatrix} B_{11} & B_{12} & B_{13} \\ B_{21} & B_{22} & B_{23} \\ B_{31} & B_{32} & B_{33} \end{pmatrix} \begin{pmatrix} u_l \\ u_r \\ v \end{pmatrix} = \begin{pmatrix} T_l \\ T_r \\ -q \end{pmatrix} \quad (2)$$

When two identical cells A and B are attached as shown in Fig. 12(b), the B -matrix after their cascading has the same form as (1), it can be reduced to the same form of (2).

Next, the cascading of four (2^2) blocks needs to be discussed. When the cascading procedure described above is applied to the newly generated B matrix, the B matrix for four (2^2) cells can be obtained. This means the run time for the B matrix calculation increases by N when identical cells are cascaded for $M = 2N$ times. This technique is also applicable

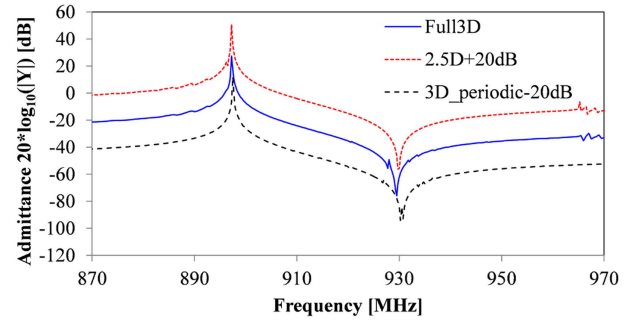


FIGURE 13. Calculated input admittance of one-port SAW resonator on $\text{SiO}_2/128^\circ \text{YX-LiNbO}_3$ structure [49].

to arbitrary integer M by its binary notation and reuse of intermediate B matrices.

Finally, the B matrix of the whole device structure can be generated by cascading multiple B matrices for all the other blocks such as PMLs at left and right ends, the input admittance Y of the target resonator can be obtained.

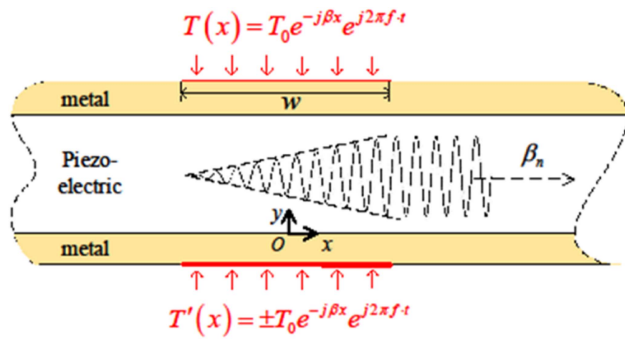
The technique is quite powerful when the device structure under concern is mainly composed of identical cells and the number of cells N is large like for SAW resonators. This is because the time consumption is almost proportional to $\log N$, while the required memory is almost independent of N . Nowadays, HCT-based 2D FEM is widely used in SAW device development.

Furthermore, other advantages exist: (a) capability to reuse intermediate results [43] to investigate variation of device characteristics with some design parameters, by running parameter scans, (b) capability to simulate semi-infinite structures [44], and (c) realization of damping mechanisms [43], [44], [45] for cases where PML does not work properly.

HCT can be also applied to 3D FEM, and demonstrated full 3D FEM analysis of practical SAW device structures [46], [47]. The authors also showed that combination of HCT with high-end general-purpose graphic-processor unit (GPGPU) makes 3D FEM simulation possible for practical SAW device structures [47], [48]. Nevertheless, applicability of full 3D is limited to relatively simple cases due to the memory size embedded in GPGPU.

Figure 13 shows calculated admittance of one-port SAW resonator using a $\text{SiO}_2/128^\circ \text{YX-LiNbO}_3$ structure [49]. Three results are shown. The full 3D simulation exhibits (a) weak longitudinal mode resonances below the resonance which also appear in the 2.5D simulation, and (b) weak transverse mode resonances near the anti-resonance, which also appear in the periodic 3D simulation. Namely, the 3D model includes scattering mechanisms included in the 2.5D and 3D periodic models. Nevertheless, the Q value for the 3D case is much lower than the 2.5D and 3D periodic cases. GPGPU of Quadro RTX 8000 (16.3 TFLOPS for FP32 with 48 GB embedded memory) was used for the calculation. Full 3D FEM took about 510 sec. per each frequency point.

HCT is also a new theoretical tool for researchers to tackle various problems on SAW/BAW excitation and scattering


FIGURE 14. Traveling wave excitation source [50].

including those believed to be impossible. An example is SAW scattering analysis at irregularity inserted in between two semi-ininitely long gratings [44] and that at IDT finger tips [48]. To the best of the authors' knowledge, such kinds of analysis have never been accomplished and reported before.

The analysis employed the traveling wave excitation source (TWES) [50]. It should be noted that HCT is easily applicable to TWES calculation without spoiling any advantages of HCT [44], [45].

Let us consider wave excitation and propagation on a plate shown in Fig. 14. A wave excitation source $T(x)$ is placed on the top surface and is driven by a sinusoidal signal with the frequency f . There can also be added another source to the bottom for selective excitation of either symmetric or anti-symmetric mode. From the law of superposition, the excited wave field $u(x)$ is given in a form of

$$u(x) = \int_{-\infty}^{+\infty} G(x-x')T(x')dx' \quad (3)$$

where $G(x)$ is the Green function proportional to $\exp(-j\beta_S|x|)$ where β_S is the wavenumber of the wave under concern.

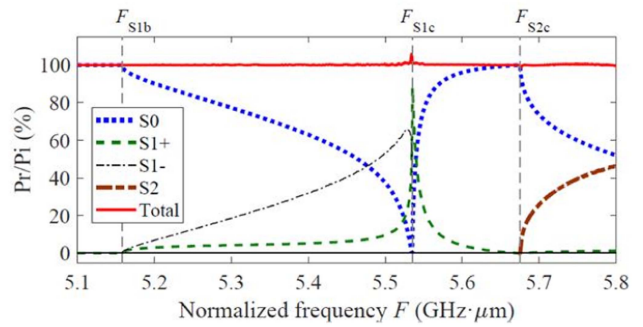
When $T(x)$ has a form of $T_0 \exp(-j\beta_T x)$, (3) can be rewritten as

$$u(x) \propto \begin{cases} T_0 w \exp(-j\beta_S x) \text{sinc}(\beta_S - \beta_T)w/2 & x \geq +W/2 \\ T_0 w \exp(+j\beta_S x) \text{sinc}(\beta_S + \beta_T)w/2 & x \leq -W/2 \end{cases} \quad (4)$$

where w is the length of the excitation source and $\text{sinc } x = \sin x/x$. Eq (4) indicates that when provided w is sufficiently large, only one mode with $\beta_S \approx \beta_T$ is predominately excited. In other words, one particular mode can be excited selectively and unidirectionally by setting $\beta_S \approx \beta_T$ provided that β_S is known for a given f in advance. TWES is not necessary to be continuous and can be an array of discrete sources. Electric sources instead of mechanical ones can also be used.

It should be noted that stress sources will not give any influence to wave propagation.

Fig. 15 shows the power scattering coefficients calculated by the TWES method when the S_0 Lamb mode is incident to the free side edge of AlN plate. In the figure, the horizontal axis is the frequency-AlN thickness product F , and F_{S1b} , F_{S1c}


FIGURE 15. Scattering behavior when the S_0 mode is incident to the free end of AlN plate [50].

and F_{S2c} are the frequencies at the cutoff for the S_{1-} , S_{1+} , and S_2 Lamb modes, respectively. The same calculation was performed by conventional FEM [51]. Although the result was similar to this, it was impure due to strong mode conversion. Note that S_{1-} mode is the backward wave, and it makes this analysis difficult. TWES can be extended to oblique incident cases [52] and SAW device structures [48] in combination with periodic 3D FEM.

VI. ADVANCES ON NONLINEARITIES MODELING AND CHARACTERIZATION

With the recent evolution of telecommunication systems, linearity performance of RF Front-end (RFFE) in mobile communication handsets becomes critical. Up-link carrier aggregation [53] is one example requiring high linearity of the RFFE. Therefore, linearity specifications for SAW and BAW filters widely used in RFFE become tighter. Under this situation, modeling and characterization of nonlinearities generated in SAW/BAW devices are one of the hottest research topics today. Accurate models are needed to understand nonlinear behaviors and to establish suppression methods for nonlinearities.

Generally, nonlinearities in SAW/BAW devices are represented by extending the piezoelectric constitutive equations based on expression of Gibbs free energy [54]. For example, the full three-dimensional extended equations in e-form are written as

$$\mathbf{T} = \mathbf{c}^E \mathbf{S} - \mathbf{e}^t \mathbf{E} + \mathbf{T}_N \quad (5)$$

$$\mathbf{D} = \mathbf{e} \mathbf{S} + \epsilon^S \mathbf{E} + \mathbf{D}_N \quad (6)$$

where \mathbf{T} , \mathbf{S} , \mathbf{D} , and \mathbf{E} are stress tensor, strain tensor, electric flux density vector, and electric field vector, respectively and \mathbf{c}^E , \mathbf{e} , and ϵ^S are elastics constant tensor, piezoelectric constant tensor, and dielectric constant tensor, respectively. \mathbf{T}_N and \mathbf{D}_N are nonlinear stress tensor and electric flux density tensor. They are represented using \mathbf{S} , \mathbf{E} , and nonlinear material constants. For one dimensional case (5) and (6) are simplified to

$$T = c^E S - e^t E + T_N \quad (7)$$

$$D = e S + \epsilon^S E + D_N. \quad (8)$$

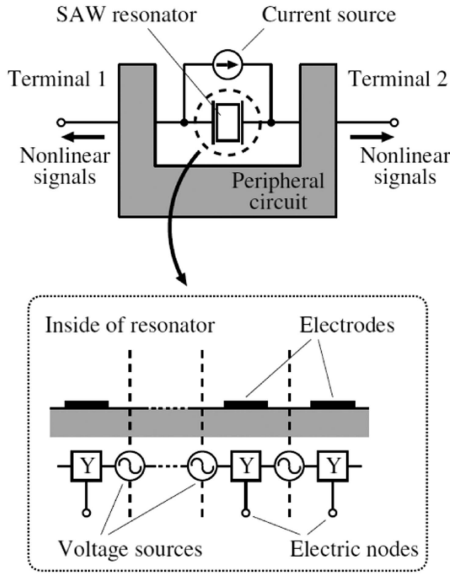


FIGURE 16. Modeling of nonlinearities in SAW using nonlinear current and voltage sources [58].

The nonlinearities modeling of SAW/BAW devices focuses on the discussion how to deal with \mathbf{T}_N and \mathbf{D}_N . In this section, several modeling techniques of the nonlinearities proposed within the last years are reviewed.

A. MODELING APPROACH FOR SAW DEVICES

Coupling of mode (COM) model [55, Chap.7] and P-matrix model [56], [57] are very popular for linear analysis of SAW devices. Therefore, for nonlinearity modeling of SAW devices, some techniques based on COM theory or P-matrix method have been proposed. In reference [58], acoustic strain S and electric field E at k -th electrode in one-dimensional model are derived using acoustic current $I_k^{(A)}$ and electric current $I_k^{(E)}$ which are obtained from the results of linear COM analysis, respectively, as

$$S_k = -\frac{j}{\omega e A_k} I_k^{(A)} \quad (9)$$

$$E_k = -\frac{j}{\omega \epsilon^S A_k} I_k^{(E)} \quad (10)$$

where A_k is an effective electrode area and ω is an angular frequency. By using S_k , E_k and experimentally determined nonlinear coefficients corresponding to nonlinear material constants, T_{Nk} and D_{Nk} are calculated.

Then, calculated T_N and D_N are given in a circuit model as shown in Fig. 16 as acoustic voltage sources V_N and an electric current source I_N , respectively. Finally, nonlinear signal levels at external terminals are estimated. The relations between T_N , D_N and V_N , I_N are

$$V_{Nk} = A_k T_{Nk} \quad (11)$$

$$I_N = j\omega \sum_k A_k D_{Nk} \quad (12)$$

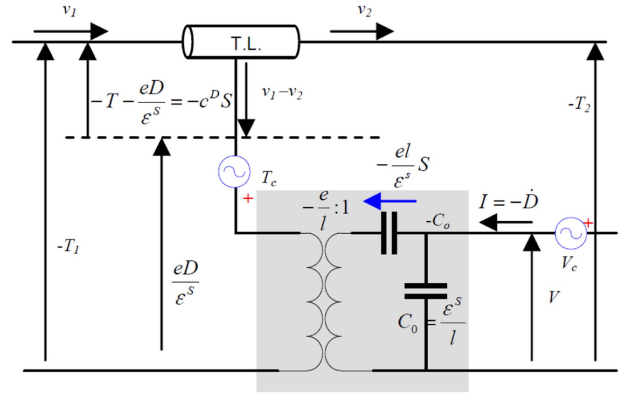


FIGURE 17. Nonlinear Mason circuit [69].

Modeling techniques based on similar approaches are also proposed in [59] and [60].

Another popular technique for modeling of nonlinearities in SAW devices is nonlinear FEM. In [61], by using S and E obtained from linear FEM analysis and nonlinear material constants, \mathbf{T}_N and \mathbf{D}_N are calculated in the form of being discretized to each element node. Calculated \mathbf{T}_N and \mathbf{D}_N are given as perturbation terms in simultaneous equations representing relations between displacement \mathbf{u} , electric potential ϕ , \mathbf{T} , and \mathbf{D} at the generated frequency of nonlinear signals. In that way the output signal is calculated. In this technique, in addition to the material nonlinearity represented by (5) and (6), structural nonlinearity can also be modeled by taking Green finite strain and Piola-Kirchhoff stress into account.

This technique might be very helpful to understand the origins of nonlinearity within a SAW device. However, while highly accurate nonlinear material constants are required for this simulation, only the constants of some materials have so far been determined [62], [63], [64], [65]. For example, the nonlinear material constants of LT being one of the most popular piezoelectric material for SAW devices have not been determined yet. Therefore, determination of nonlinear material constants is highly desired. As an interim solution scaling the constants of LN has been proposed to determine the LiTA03 constants [66].

B. MODELING APPROACH FOR BAW DEVICES

For linear analysis of BAW devices, Mason's equivalent circuit model is one of the most popular techniques [67], [68]. By extending this model to nonlinear form, generation of nonlinear signals in a BAW device is represented as Fig. 17 [69]. In this nonlinear model, T_c and V_c are nonlinear acoustic and electric voltage sources, respectively, and they are represented using T_N and D_N in (7) and (8) as

$$T_c = T_N + \frac{e}{\epsilon^S} D_N \quad (13)$$

$$V_c = \frac{1}{\epsilon^S} \int_l D_N dx \quad (14)$$

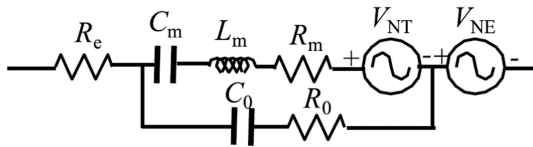


FIGURE 18. BVD model including nonlinear signal sources [71].

where l is thickness of piezoelectric film. In [69], the nonlinear Mason model in Fig. 17 is analyzed using the harmonic balance solver implemented in commercial circuit simulators such as Keysight ADS. Another popular technique for nonlinearity modeling of BAW devices is also the nonlinear FEM [70]. This model is mainly used to take effects of spurious modes into account. In reference [70] to calculate harmonic modes, four weak form equations including nonlinear effects are prepared as

$$\int_{\Omega} (\rho \omega_n^2 u \tilde{u} - T \tilde{S} + D \tilde{E}) d\Omega + \int_{\Omega} (-T_N^{(n)} \tilde{S} + D_N^{(n)} \tilde{E}) d\Omega = 0, \quad (15)$$

where ω_n ($n = 0, 1, 2, 3$) correspond to the frequency of DC, fundamental, second and third order harmonic, respectively. $T_N^{(n)}$ and $D_N^{(n)}$ are contributions of nonlinearities at each frequency. \tilde{u} , \tilde{S} , and \tilde{E} correspond to FEM test functions. The equations are solved simultaneously using damped Newton iteration method implemented in commercial FEM simulator COMSOL.

In addition to above mentioned two techniques, a nonlinearity modeling technique of BAW devices using perturbation analysis based on mass-spring model is also proposed [71]. In this technique, one-dimensional h-form piezoelectric constitutive equations:

$$T = c^D S - h D + T_N \quad (16)$$

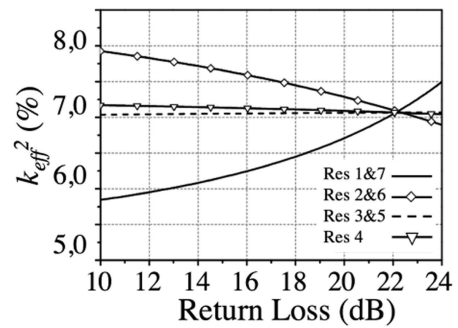
$$E = -h S + \beta^S D + E_N \quad (17)$$

are used instead of those in e-form to satisfy uniformity of electric flux density in piezoelectric films. Nonlinear terms T_N and E_N in (16) and (17) are calculated using S and E obtained from linear Butterworth van Dyke (BVD) model, and then, they are given in the BVD model as an acoustic voltage source V_{NT} and an electrical voltage source V_{NE} as shown in Fig. 18. V_{NT} and V_{NE} when thickness of piezoelectric film is l are represented as

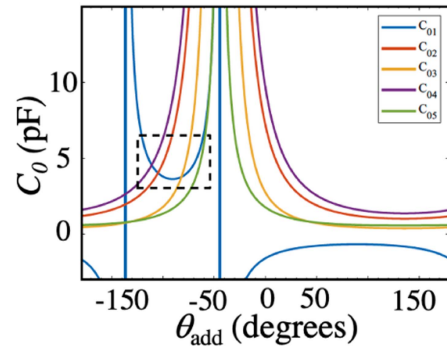
$$V_{NT} = -\frac{\beta^S l}{h} T_N \quad (18)$$

$$V_{NE} = -l E_N. \quad (19)$$

In this technique, influence of spurious modes to nonlinear response can be easily considered since the spurious mode responses are represented by adding extra acoustic branches to the normal BVD model. Furthermore, a black box modeling technique (similar to S-Parameters for the linear regime) -



(a)



(b)

FIGURE 19. (a) Value for the k^2 of each resonator in a 7th order Ladder filter as a function of RL for a given set of transmission zeros [74]. (b) Dependence of the static capacitance C_0 with the input phase of the filter [77].

the Polyharmonic Distortion Modeling has been used [72] with according measurement set up [73]. The advantage of the black box modeling approach is that no device physics knowledge is required and it can be easily exchanged between different suppliers without the concern about intellectual property.

VII. SYNTHESIS METHODOLOGIES FOR ACOUSTIC WAVE FILTERS

The complexity of the requirements in advanced 5G and forthcoming scenarios has a direct impact in the design of an acoustic wave filters. Latest developments have pushed acoustic technology to an unprecedented situation, however, this must be accompanied by new synthesis methodologies as an essential tool for: speeding up the design process instead of conventional optimization methods and explore new filter configurations which may overcome today's barriers. In this section, some examples are shown where the synthesis methodologies provide the understanding to bring the design of acoustic wave filters beyond the state-of-the-art.

The synthesis methodology in [74] is based on the classical extracted pole technique [75] which be applied to the case of acoustic wave resonators for a conventional ladder-type filter. The exact synthesis methods allows to precisely analyze important features as the one in Fig. 19(a). It can be seen that for a specific set of transmission zeros, there is one single

value of return loss ($RL = 22$ dB) in which all resonators present the same k^2 , therefore, no external reactive elements are required to accommodate technology constraints. It also allows to explain and propose solutions to common problems as it is the case of the transmission response degradation due to electromagnetic feedthrough through the package [76] which cannot be overcome using optimization methods.

These methodologies are also useful in order to optimize, not only the performance of the filter, but also the size. From this point of view, although it is not common to put the attention on it, the input phase of the filter plays a key role. It can be set in such a way no input/output reactive matching elements are required when designing a stand-alone filter. In the case of a duplexer, it can be set, for each channel, to force an open-circuit condition at the counterband so reactive loading effects are minimized. Moreover, the input phase of the filter is also related to the total static capacitance of a filter as shown in Fig. 19(b). It is seen that the capacitance value for each resonator depends on the input phase of the filter which lead to a new design degree of freedom very valuable since the total size of the filter is expected to be reduced as much as possible.

The curves in Fig. 19(b) show cases where the capacitance values are negative as it is the case of the first series resonator for input phase values around -150 degrees. This is an undesired condition since the acoustic wave resonator require a positive static capacitance C_0 . Taking advantage on the synthesis methodologies, this can be used in order to alter the classical alternation of transmission zeros above and below the passband giving by the series and shunt resonators respectively [77], [78]. The value of the frequency invariant reactance is related to the allocation of the transmission zero. Taking this into consideration, for a given input phase leading a negative capacitance, the transmission zero can be allocated in the opposite expected side of the passband, that is a series resonator contributing with a transmission zero below the passband (expected by a shunt resonator) or a shunt resonator contributing with a transmission zero above the passband (expected by a series resonator). This situation is depicted in Fig. 20 where the transmission response for a 5th order filter is shown. Since the first resonator is series, it would be expected to observe three transmission zeros above the passband and two below. However, in this case, the first series resonator contributes with a transmission zero below the passband which can be used as a solution to improve the rejection level without the need of increasing the number of resonators while its static capacitance C_{01} is positive as depicted with the dashed box in Fig. 19(b).

The proposed synthesis methodologies can be also applied to the design of multi-band filters. In [79], the synthesis for designing a dualband inline filter was proposed. This configuration is based on the electrical connection of basic dual cells composed of two series and two shunt resonators as shown in Fig. 21(a). Again, the input phase plays a critical role to success in the synthesis since it must be define in such a way two transmission zeros can be extracted simultaneously.

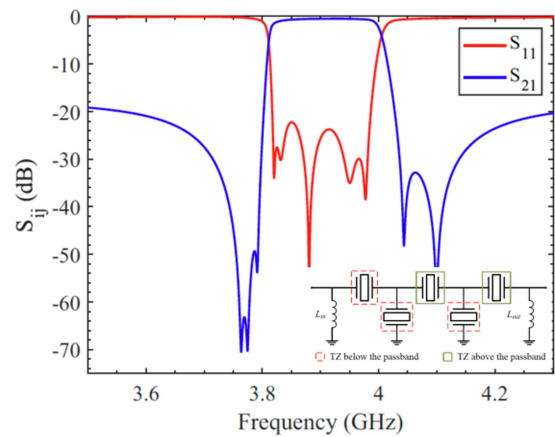


FIGURE 20. 5th order Ladder-type filter starting with series resonator. The first series resonator contributes with a transmission zero below the passband [77].

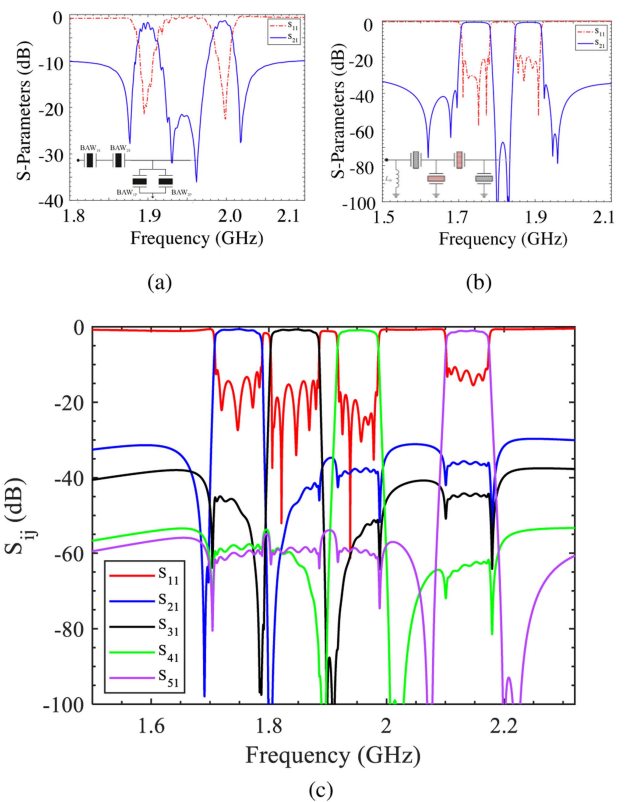


FIGURE 21. (a) Co-simulation using measured acoustic resonators for a Double-Ladder topology [79]. (b) DualBand response using a single standalone Ladder type configuration for the Uplink B66/B25 bands [81]. (c) B1-B3 Rx-Tx Bands and independently controlled RL.

To this aim, an asymmetric mapping formula solution was developed in [80], however, the drawback is the limitation on having homogeneous k^2 in all the resonators. As an alternative, in [81], a dual-band filter is proposed based on a classical ladder configuration as depicted in Fig. 21(b). Although the

sorting of the transmission zeros to be extracted is very important to obtain a feasible solution, there is no restriction on the input phase of the filter and homogeneous electromechanical coupling constant can be obtained in all resonators.

The synthesis methodology can be extended to multiplexers with arbitrary number of bands, as demonstrated in [82]. The idea behind this work is to obtain the predistorted characteristic polynomials of individual channels in such a way when they are connected in a star-junction configuration, the resulting transfer function of the whole multiplexer is equiripple, with independent control of the RL level at each channel. As an example, in Fig. 21(c) a B1-B3 quadplexer is found where the RL has been defined to be different at each channel. Since each individual transfer function is not equiripple, this may present complex reflection zeros instead of pure imaginary. The extracted pole method is not able to deal with complex reflection zeros, however, this limitation can be overcome with the use of rotation of the coupling matrix in order to carry out the extraction [83]. Nevertheless, it has to be highlighted that the exact analytical solution highly reduces the required computation and/or optimization time to face the design of a multichannel configuration.

VIII. TUNABLE AND RECONFIGURABLE ACOUSTICS

Today's cell phones employ many filters and switches. The number of acoustic filters in cell phones is expected to exceed one hundred in the near future [84] contributing to mobile device rising cost and size. Besides approaches in filter miniaturization to accommodate a large number of filters in a small RF frontend, tunable and reconfigurable acoustic filters can alleviate the above challenges by enabling a single filter to operate within multiple frequency bands. In this section an overview of recent research in the design of high performance switchable and reconfigurable BAW and SAW filter technologies is given. For example, [85], [86], [87], [88], [89], [90] describe research on the design of tunable and reconfigurable acoustic filters by incorporating switches as well as varactors within the acoustic devices. Another attractive approach is to integrate both switching and filtering functionalities onto a single device instead of the combination of switchplexers and conventional BAW filters. This can be achieved with intrinsically switchable acoustic filters based on thin film ferroelectrics such as barium strontium titanite (BST) as well as ScAlN FBARs.

BAW resonators based on ferroelectric BST exhibit several interesting features, allowing potential simplification of RF frontends. Due to BST's strong electrostriction properties, BST resonators can be switched on and off with the application of a DC bias voltage [91], [92], [93], [94], [95], [96], [97], [98], [99], [100], [101], [102], [103], [104], [105]. A photograph of an intrinsically switchable BST FBAR is shown in Fig. 22. Measured reflection coefficient of such a device is plotted on Smith chart in its ON and OFF states are provided in Fig. 22. As shown in this figure, the device in its OFF state behaves like a simple capacitor. Applying a DC bias voltage across the resonator turns on the piezoelectricity,

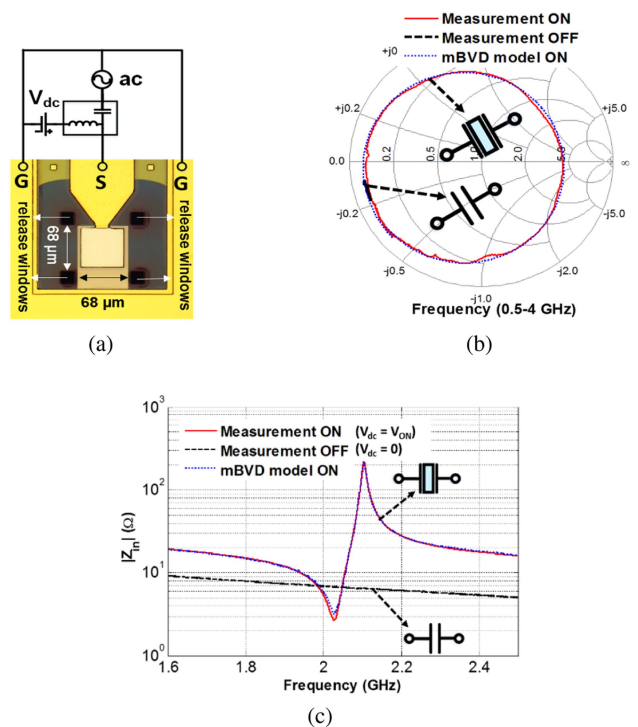


FIGURE 22. (a) A BST Switchable FBAR. (b) Reflection coefficient (c) magnitude of input impedance for the measured 1-port switchable BST FBAR in its ON ($V_{dc} = 70$ V) and OFF states ($V_{dc} = 0$ V) [100].

allowing the device to behave like a resonator; k^2 of 8.6% with a mechanical quality factor Q_m of 360.

Switched-mode reconfigurable ferroelectric based acoustic resonators have also been recently introduced [106], [107], [108]. Switched mode acoustic resonators containing multiple layers of half wave ferroelectrics can operate at different frequency bands without compromising k^2 [108]. Such resonators can be used to design switchable band filters for RF frontends. By providing appropriate bias voltages across the ferroelectric layers, they selectively operate at different eigenmodes of the acoustic resonator. The applied bias fields determine the magnitude and sign of the piezoelectric coefficient in each ferroelectric thin film (the slope of the u-E in Fig. 23(b)). An appropriate DC bias configuration turns the desired resonance mode on while other modes are being suppressed. A dual resonance switched mode ferroelectric FBAR is demonstrated in [108], where the resonator consisting of two BST layers (Fig. 23(a)) can selectively resonate at its fundamental mode in 2 GHz band depicted as mode 1) or its second harmonic mode (3.6 GHz band shown as mode 2). The DC bias voltage configuration for each mode is shown in Fig. 23(a). The structure of the fabricated device and its impedance response are provided in Fig. 23(b) and (c), respectively. As shown in this figure, when either of modes is selected, the other mode is fully suppressed, and the device is switched off without DC bias.

Switchable contour (lateral) mode resonators have also been investigated. The resonance frequency of contour mode

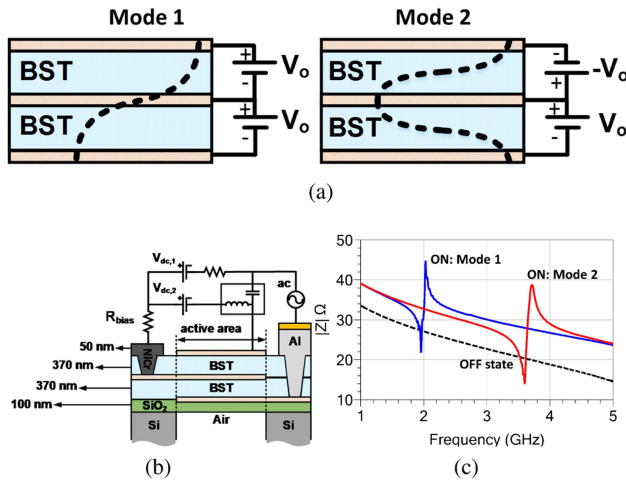


FIGURE 23. (a) Simplified structure of a dual-band switched-mode ferroelectric FBAR in mode 1 and mode 2 with their corresponding DC bias voltage and the standing wave strain field distribution. (b) The cross-sectional view of the fabricated devices and the measurements setup as well as (c) the measured impedance response of the resonator in each mode along with its OFF state [108].

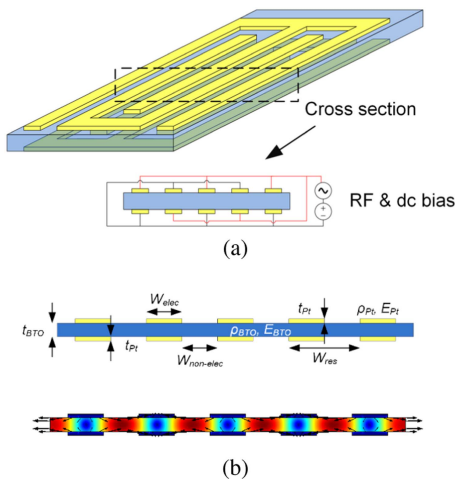


FIGURE 24. (a) TFE contour mode interdigitated resonator and (b) corresponding strain fields in ON state simulations.

resonators is determined through the lithographical process, allowing a large number of resonators with varying resonance frequencies to be realized on a same wafer without increasing the number of processing steps. Ferroelectric barium titanate (BTO) is used in the design of contour mode resonators due to its non-zero effective d_{31} piezoelectric coefficient when polarized by an external electric field. This property allows for the excitation of laterally propagating acoustic waves within the resonator (ON state). Without bias voltage, resonance can be switched off. Further increasing the DC bias voltage leads to polarization in the opposite direction to the original polarization and a strong piezoelectric response due to BTO's large electrostriction coefficient. Interdigitated contour mode resonators are designed as either thickness field excitation (TFE)

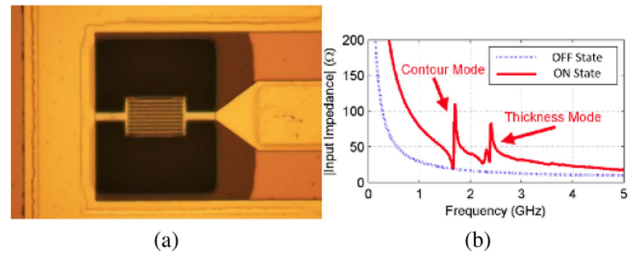


FIGURE 25. (a) Photograph of a fabricated BTO based TFE contour mode interdigitated resonator and (b) its impedance response in ON and OFF state [103].

or lateral field excitation (LFE) devices. In TFE resonators, the electric field vectors are approximately perpendicular to the plane of the thin film, and in LFE resonators, the electric field vectors have a component parallel to the plane of the thin film. An example of TFE interdigitated contour mode resonators, which excites under the application of an RF signal and DC bias to the interdigitated electrodes is shown in Fig. 24 [103].

Simulation of the contour mode resonator, shown in Fig. 24(b), indicates that the resonance frequency is determined by the width and spacing of the interdigitated electrodes and resonator's material property. A photograph of a fabricated intrinsically switchable interdigitated lateral mode resonator, as well as its impedance response in ON and OFF states, is shown in Fig. 25 where they can be used as a building block for multi-frequency switchable filters.

Application of intrinsically switchable resonators in design of a quad band intrinsically switchable filter bank has been demonstrated [105], where four parallel filters based on BST FBARs, operating across neighbouring frequency bands are fabricated. Each filter can be switched on or off by applying DC voltage at their respective nodes (see Fig. 26).

Figure 26(b) depicts a photograph of the fabricated reconfigurable quad band FBAR filter bank, with a total active area of $340 \mu\text{m} \times 840 \mu\text{m}$. The filter's transmission is shown in Fig. 26(c). It provides reconfigurability through DC bias control across four 2.5 stage BST FBAR filters with IL ranging 6-7 dB and out of band rejection 30 dB. When all filters are off, the filter also provides about 30 dB of rejection.

Furthermore, the first demonstration of reconfigurable acoustic RF filters based on a combination of switchable BST FBARs and lumped components providing a unique reconfigurable transfer function characteristics and enhanced fractional bandwidth has been presented in [109].

IX. MILLIMETERWAVE ACOUSTICS

Demand for wireless data is growing at an astounding rate of 30% a year. Current wireless infrastructure cannot accommodate this growth rate. The 5th Generation (5G) cellular network technology is meant to address these needs by enabling communication data links in the millimeter wave

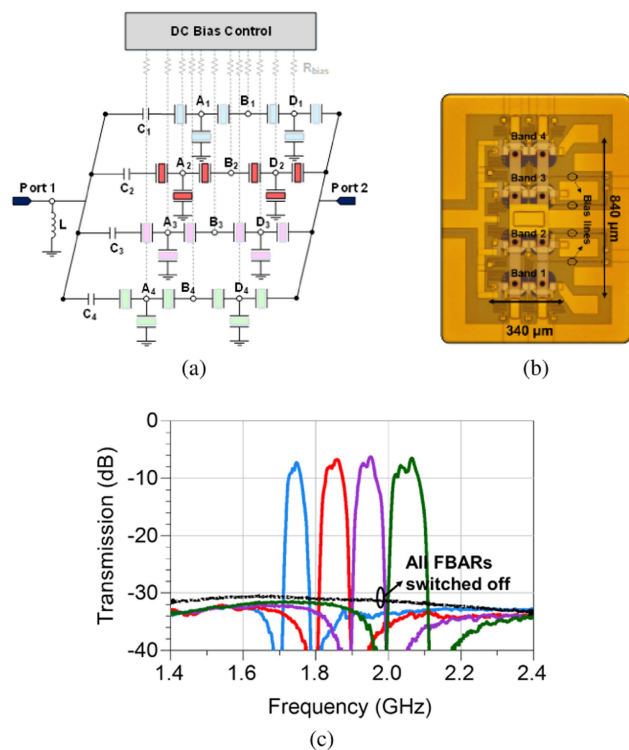


FIGURE 26. (a) Schematic of a quad band intrinsically switchable BST FBAR filter bank. DC biasing network and (b) the photograph of the fabricated structure [105].

(mmW) range (around 30 GHz, 40 GHz, and 60 GHz) using phased arrays. 5G is meant to revolutionize the way we communicate by facilitating high speed data links for augmented and virtual reality, unmanned air vehicles and self-driving cars, remote health and infrastructure monitoring, and the Internet of Everything. As the number of deployed 5G systems will increase, the number of bits required by the baseband analog-to-digital converter (ADC) of each channel (or element in the phased array) is going to be limited by the interference levels. Anticipating that filtering will be essential in limiting the ADC power consumption for each element in the phased array as well as reducing the linearity requirements on the amplifiers. The needs for mm-wave filtering will become a fundamental bottleneck to further deployment of 5G networks. The design and implementation of bandpass filters at these frequencies in the form factors required by on-chip, portable and wearable devices is particularly challenging. Proposing a disruptive vision in which sharp filtering can be performed directly at each antenna element in a form factor much smaller than the half-wavelength separation between adjacent antenna elements using acoustic resonators.

In this section, state-of-the-art in regards to mm-wave microacoustic resonators and outline key bottlenecks for attaining high performance at these frequencies are reviewed. An innovative design that will permit to attain high k^2 and Q at mm-wave frequencies is also presented. Because of the

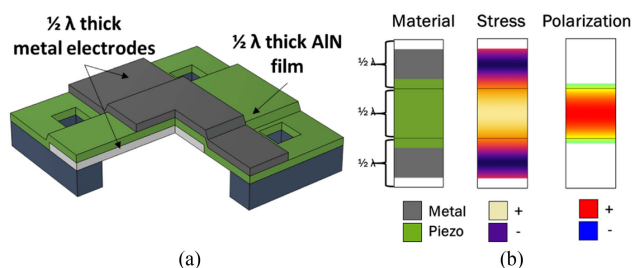


FIGURE 27. Graphs of k^2 - Q product vs. frequency for some classes of acoustic resonators demonstrated above 10 GHz. Trends highlight degradation in performance vs. frequency. Investigations in materials and design paradigm changes are needed to disrupt these trends.

specific mode of operation of this design, it is dubbed the overmoded bulk acoustic resonator (OBAR).

A. OVERVIEW OF MM-WAVE ACOUSTIC RESONATORS

Various technologies for performing filtering functions at mm-wave frequencies have been demonstrated. These techniques are all based on the use of electromagnetic resonators. Whether waveguide resonators, low-temperature co-fired ceramic cavity resonators, loaded cavity resonators, microstrip filter resonators, or laminated core resonators are used, the filter dimensions are fundamentally limited by the size of the electromagnetic wavelength at these frequencies. The smallest demonstrated filters at 5G frequencies exceed 1/2 of the electromagnetic wavelength, rendering impractical their insertion at each antenna element (which are also generally spaced by 1/2 of the electromagnetic wavelength). Acoustic resonators, by virtue of a much smaller phase velocity (a few thousands m/sec for acoustic waves vs. $\approx 10^8$ m/sec for electromagnetic waves), enable extremely small form factors at mm-waves (potentially only a few microns on a side per device) and are likely to be the only viable approach for the implementation of direct filtering at each antenna element in a phased array.

The design of an acoustic resonator should aim at: 1) attaining a high electromechanical coupling, which facilitates the synthesis of low loss and wideband filters; 2) achieving high Q to minimize filter losses and ensure steep roll-off; 3) demonstrating impedances matched to 50 Ω in a small form factor so as to minimize the need for external matching components.

Earlier work on 10-50 GHz acoustic resonators has shown that it is feasible to demonstrate vibrating mechanical devices operating in the mm-wave frequency range (Fig. 27). Work on piezoelectric aluminum nitride resonators by Fujitsu [110], [111] shows that 28 GHz resonators can be demonstrated in nanoscale films and very small form factors (just few microns on a side). These devices could be matched to 50 Ω , but suffered from relatively large losses and the demonstrated quality factors (Q_s) were below 200, making them far less competitive with respect to alternative electromagnetic-based filtering technologies in terms of resulting filter losses and roll-off. Works by the MEMS community [112], [113], [114], [115],

[116], [117] have confirmed that the same AlN films or doped films can operate at these frequencies and in topologies, which support either higher quality factors ($Q \approx 500$) or large coupling ($k^2 \approx 10\%$). The integration of resonators in advanced CMOS processes [118] has facilitated the insertion of innovative phononic crystal designs into electrostrictive acoustic resonators, which have exhibited exceptionally high- Q in excess of 10,000 at mm-wave frequencies. The low electromechanical coupling intrinsic to the electrostrictive transducer renders the device characteristic impedance very high and most importantly limits the attainable filter bandwidth, making such device impractical for 5G filtering applications. However, this demonstration clearly shows that high- Q at mm-wave is possible. The exploration of alternative ferroelectric thin films made available by atomic layer deposition such as HfO_2 have enabled the demonstration of mm-wave vibrations in various resonator geometries [119], [120]. Despite the progress, these devices still suffer from large impedances and high losses limiting their Q s to be below 300 at the highest frequencies. Recent work on over-moded acoustic resonators in thin films of LN [121], [122], [123], [124], [125] has shown that these devices can support frequencies up to 50 GHz with Q s in the order of a few 100 s. Despite the acceptable electromechanical coupling, the method of excitation of these modes of vibrations make it impractical to attain the desired characteristic impedances in a competitive form factor or ways that would ensure accurate frequency setting.

Existing demonstrations of microacoustic resonators at mm-wave show that there are various materials that can support acoustic vibrations at mm-wave, but we are still far from delivering devices that simultaneously attain a high quality factor ($Q > 1,000$), a characteristic impedance that can be readily interfaced with 50Ω and the desired filter bandwidth, let alone the suppression of undesired spurious vibrations. Fundamental investigations in innovative acoustic resonator designs and materials that support the desired k^2 and Q s at mm-wave frequencies are needed to disrupt the trends exhibited by the state-of-the-art.

B. THE OVERMODED BULK ACOUSTIC RESONATOR

The use of BAW resonators in their fundamental extensional modes beyond 30 GHz results in metal and piezoelectric layers with thicknesses that are not practical to manufacture. Furthermore, the losses from the resistance of resonator electrodes become prohibitively large with frequency reducing the device Q .

In [126] for the first time, an Overmoded Bulk Acoustic Resonator (OBAR) (Fig. 28) for mm-wave acoustic filtering was presented. This device allows using more practical film thicknesses, minimizes electrical loading due to electrode resistance and does not sacrifice k^2 . The OBAR functions in a 2nd overtone thickness mode evenly split between the piezoelectric and electrode layers allowing a k^2 of up to 2/3 of the fundamental mode.

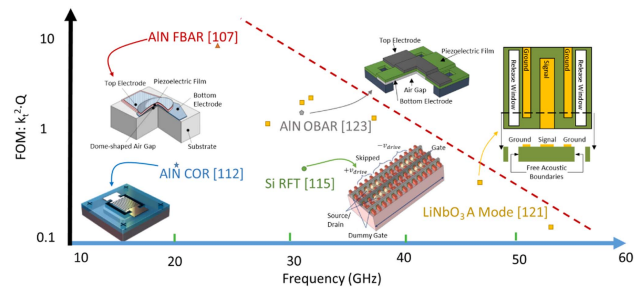


FIGURE 28. (a) 3D rendering of the OBAR devices formed by a piezoelectric layer sandwiched between two metal layers each having a thickness comparable to 1/2 of the acoustic wavelength in the material. (b) graphical representation of the mode of vibration across the film stack showing how stress is distributed equally across the 3 layers and max uniform polarization is attained in the piezoelectric layer [110], [115], [118], [124], [126].

1) PRINCIPLE OF OPERATION AND DESIGN

The OBAR (Fig. 28) functions in a 2nd overtone, but instead of confining acoustic energy solely in the piezoelectric layer, the mode is split evenly between the piezoelectric layer and each electrode. The piezoelectric layer and each electrode have thicknesses approximately equal to 1/2 the acoustic wavelength (λ), ensuring that maximum energy is coupled in the piezoelectric layer. This prevents the typical problem of overtones in which regions of expansion and contraction produce positive and negative polarizations which cancel net charge, thereby reducing k^2 .

An OBAR distributes acoustic energy between the piezoelectric layer and electrodes, so the use of high acoustic impedance (Z) electrodes to confine energy in the piezoelectric layer is detrimental. Instead k^2 can be maximized by minimizing the acoustic load from the electrodes—meaning low Z electrodes are preferable. The OBAR can be synthesized using different piezoelectric materials, such as AlN, ScAlN, LT or LN. The use of higher intrinsic coupling material will directly favour the synthesis of devices with higher k^2 . The metal electrodes should be optimized specifically for each piezoelectric material, but material such as Al or Ti should be preferred over W or Mo.

2) EXPERIMENTAL DEMONSTRATION AND CONSIDERATIONS

The OBAR reviewed in this work, has lateral dimensions of $14 \mu\text{m} \times 14 \mu\text{m}$ ($196 \mu\text{m}^2$) in order to be approximately 50Ω matched. The stack consists of a 70 nm Pt bottom electrode with 10 nm Cr adhesion layer, 140 nm AlN piezoelectric layer, and 90 nm Al top electrode. The material selection was driven by ease of fabrication and not by the goal of maximizing coupling or Q .

The fabricated OBAR was measured on an Agilent PNA-X in a thru configuration using two $150 \mu\text{m}$ pitch GSG probes. The characteristic admittance response of this device is shown in Fig. 29. Measured k^2 of 1.7% is 20% lower than FEM simulated value of 2.1% which may be due to discrepancies in material properties between the simulated and sputtered

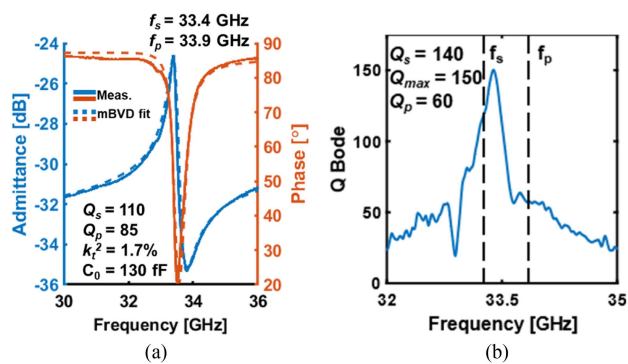


FIGURE 29. (a) Admittance response of one of the demonstrated 33 GHz OBAR devices. (b) Bode Q_{Bode} plot for the same device highlight the behavior of Q vs. frequency [126].

films. While there is some difference in the values of Q between Q_{Bode} and the mBVD fit, both show Q at series resonance above 100. This is below the Q of 290 reported by [111], but the electrode stack was not optimized in the current work. Losses are also currently higher than what can be accomplished with transmission line approaches implemented in CMOS fabs [127]. However, the analysis shows that appropriate material selection and further optimization of the fabrication process will yield miniaturized devices with significantly improved k^2 (10%) and Q (> 500).

X. OSCILLATORS

Quartz crystal oscillators have dominated the timing reference market for almost a century since their invention in the 1920s [128]. These crystal oscillators have found utility in a wide range of products from low-end (real-time clock) to high-end (GPS, military, and aero) applications due to their excellent frequency accuracy, low phase noise, low temperature drift, and good long-term stability. The emerging mobile communication and electronization of various industries, e.g. electric vehicles and IoT, have driven the search for new timing technologies which consume lower power, with smaller form factor for integration, and ready for mass production. With the phase velocity in the order of several thousands of meters per second, micro-acoustic resonator technologies have been proven as promising solutions to realize high- Q devices in compact sizes for this purpose [129]. In this section oscillators using BAW for timing are reviewed.

A. WHY BAW FOR TIMING

Various novel oscillator products utilizing non-crystal frequency sources, either capacitively or piezoelectrically driven, have been successfully released to the market since 2006 [129], [130], [131], [132], [133], [134], [135]. Among them, the BAW resonator technology capable of generating high- Q ($> 1,000$) and high-frequency (> 2 GHz) resonance is a unique candidate for the timing application. Although the RF filter applications require the composing resonators to be operated at different frequency bands of interest, the selection

of frequency for micro-acoustic resonators is more flexible for timing because after all the system would require extra circuits to sustain the oscillation and to compensate the drift over temperature. Unlike low-frequency crystals or MEMS oscillators which require PLLs (phase-locked loops) to generate higher output frequencies, oscillators based on gigahertz BAW resonators rely on the usage of FODs (fractional output dividers) to generate output frequencies from tens to hundreds of megahertz as it provides the balance between low jitter and compatible power consumption. However, this performance-power balance vanishes for applications requiring kilohertz output frequencies (e.g. RTC) because the divider power consumption could exceed that of the core oscillator block. At this frequency range, utilizing low-frequency MEMS resonator technologies (capacitive resonator, or piezo-on-Si technology) is more suitable [130], [131], [133], [134].

B. OSCILLATOR ARCHITECTURE

An oscillator circuit is used to provide the required energy and compensate the losses to sustain the oscillation of the system. The frequency of the oscillator should be mainly defined by the frequency of the high- Q resonator so the perturbations from circuit or environment are minimized [136]. Different oscillator architectures have been used as the sustaining circuitry. The Pierce oscillator is the simplest architecture which can be implemented with only one transistor and two functional capacitors [128]. However the non-symmetrical architecture hinders its usage in RF applications which usually prefer symmetrical signals. Symmetrical oscillator architecture can be categorized by operating at the resonator's series-resonance frequency (f_s) or at the parallel-resonance frequency (f_p). Various oscillator studies based on the BAW technology have been demonstrated [137], [138], [139], [140], [141]. In order to achieve low-power consumption, the oscillator cores in [140], [141] employed the complementary cross-coupled differential architecture operating around the parallel resonance f_p of the dual-bragg acoustic resonator (DBAR). Besides the power advantage, this implementation also provides the flexibility to add inductance (longer routings) in series with the DBAR to improve the tuning range without affecting the operation frequency. The increase of electrode routing length in this configuration also has minimum impact on the Q at parallel resonance (Q_p), which is important for the package stress isolation.

C. FREQUENCY ACCURACY CONTROL

Since the resonance frequency of a BAW resonator is determined by the film thicknesses used in the stack, process non-uniformity could introduce undesired cross-wafer and cross-lot frequency variations. The ion-beam trimming is a commonly used technique to tighten the distribution of BAW frequencies to about $\pm 1,500$ ppm with a reasonable fabrication cost. Although this ± 500 ppm out-of-fab frequency offset is sufficient for most of the filter applications, additional active accuracy control (or calibration) is required for the timing applications. One commonly used approach is to connect the

BAW resonator in parallel with a tunable capacitor bank, and use that to pull (in this case, f_p of the resonator) and calibrate the oscillator frequency directly. Alternatively, one can use a high-resolution FOD to divide and calibrate the oscillator to the desired output frequency. In this case, the overall jitter of the oscillator would be dominated by the performance of the FOD. In either approach, the programmability or tuning range must be able to cover above mentioned out-of-fab frequency offset with a good resolution.

D. SHORT-TERM STABILITY

Frequency stability of an oscillator can be categorized into short-term, which is usually measured at rates less than one second and has a random nature (e.g. amplifier flicker noise), and long-term, which is relatively slower and has a deterministic nature [142]. Temperature is one of the most prominent factors affecting short-term stability of an oscillator. To solve this issue, the quartz and SAW communities utilized different orientations, also called cuts, to alter the direction of acoustic wave propagation and achieve different thermal stability and aging characteristics. On the other hand, silicon resonator technologies, either employ piezoelectric or capacitive transductions, are using degenerate doping to achieve promising passive temperature compensation results [143], [144]. However, either technique is applicable to thin film-based BAW resonators. AlN thin film BAW resonator could encounter 3,000 ppm frequency drift across the industrial temperature range ($-40\text{ }^{\circ}\text{C}$ to $105\text{ }^{\circ}\text{C}$) due to its 1st-order TCF of about -25 ppm/K . Although this number is much smaller compared to the TCF of LiNbO_3 or LiTaO_3 used in the SAW technology, the resulted frequency drift across the entire temperature range is still too large to be compensated using a digital compensation scheme at circuit level directly. A passive temperature compensation technique at material or device level is therefore required. Inserting a correct amount of silicon dioxide layer (temp-compensation oxide) in the BAW resonator stack is a well-known technique to reduce the 1st-order TCF of the BAW resonator [145]. It is due to the mechanical stiffening behavior of SiO_2 at elevated temperature (a positive TCF). In [129], [145], the 1st-order TCF of the BAW resonators is passively compensated to less than 1 ppm/K , reducing the overall frequency drift from 3,000 ppm to less than 200 ppm across $-40\text{ }^{\circ}\text{C}$ to $105\text{ }^{\circ}\text{C}$. Note that the turnover temperatures of these passively compensated BAW resonators shall be engineered near the operation temperature at which the drift is minimum. Subsequently, the temperature characteristics of these passively compensated BAW resonators can be captured using a multi-temperature insertion at the final test for further active compensation to the required stability level for different protocols. Active temperature compensation of a BAW-based oscillator can be achieved at circuit level by utilizing a look-up table (LUT) which stores the fitted correcting code collected during final test across selected temperatures [140], [141]. Due to its small 3rd-order TCF, the temperature behavior of passively compensated BAW resonators can be characterized with 3 temperature insertions and

fitted as a quadratic equation. Referencing the readings from the temperature sensor, the system can continuously perform output frequency correction using a fractional-PLL [140], an FOD [141], or dialing a fine-resolution capacitor bank with pre-stored compensation codes. As a result, an oscillator with less than $\pm 4\text{ ppm}$ stability across $-40\text{ }^{\circ}\text{C}$ to $85\text{ }^{\circ}\text{C}$ is demonstrated [141]. This number leaves an ample margin for other frequency drifts and could address most requirements for the BLE protocol ($\pm 40\text{ ppm}$), standalone oscillators ($\pm 25\text{ ppm}$), or even sub-GHz applications. More aggressive higher order fitting algorithm paired with a fine-resolution local temperature sensor can further improve this stability at the expense of final test cost.

E. LONG-TERM STABILITY

On the other hand, oscillator's long-term stability, aging, is defined as the frequency drift over time. Typically the aging requirement of an oscillator product is application-dependent which can range from tens of ppm (e.g. local-area wireless standards [146]) to less than one ppm (e.g. LTE communications [147]). Qualifying a new resonator technology requires measuring its aging through the entire life of the product, typically 10 years. Since this is impractical, accelerated aging involving measurement at higher temperatures has been adopted by the industry as an alternative procedure [148]. This procedure tracks oscillator aging at certain temperatures and simply extrapolate the frequency drift to the time of interest. However this approach is purely experimental, statistic-heavy, and lacking of physical explanations. In [149] Segovia-Fernandez et al. presented a novel accelerated aging test method based on the time-temperature superposition principle. The method models the relaxation of viscoelastic materials and their impact to package stress over time, then uses this information to predict the aging of DBAR oscillators. Extensive aging studies proved that most of the DBAR oscillator aging is originated from the package-induced stress. In [150] Sridaran et al. presented an FBAR-based oscillator and also pointed out the undesired package stress impact on the output frequency stability. Unlike capacitive micro-resonators with which the resonator body can be supported by a single anchor, or isolated by trenches from rest of the substrate, piezoelectric resonators usually have stronger stress coupling to their substrates and require electrode routings directly connected to the resonator body. Therefore, they are more susceptible to package-induced stress and aging. To overcome this challenge, comprehensive stress simulation and package integration were implemented to isolate the DBAR from its package [151]. As mentioned previously, operating the oscillator at the parallel resonance allows longer routing for stress isolation without affecting the oscillator output frequency.

F. CHALLENGES TOWARDS COMMERCIALIZATION

The key to a commercialize oscillators based on micro-acoustic resonator technology is to find a balance among performance, power consumption, form factor, and cost.

Among them cost is usually what the customers care the most. For MEMS production, testing and packaging could account for more than 60% of the total cost. In [129] demonstrated a DBAR co-packaged with a BLE die in a 7.0 mm × 7.0 mm QFN package. The utilization of dual-Bragg acoustic mirrors under and above the resonant body effectively reduced the frequency sensitivity to contamination and humidity, allowing cost-effective non-hermetic packages. The high-frequency nature of micro-acoustic resonators also allows the implementation of the multi-tone testing configuration [152] which significantly reduces the testing cost in mass production.

XI. CONCLUSION

So, what is next? Judging from the last 30 years, we can expect significant breakthroughs for both SAW and BAW devices sometime in the next decade. One speculation can be that filters - like transistors - will one day be integrated on a single die. A more prosaic need is to continue to develop filters that remain linear and 'unruffled' by large input power. Power handling will drive filter technology - simply because higher power gives a better signal to noise ratio in cell phones and reduces the need for more base stations.

The acoustic filters based on XBARS combine low loss, wide relative frequency bandwidth and steep skirts. If remaining problems - frequency trimming, power handling increase and mechanical robustness - are solved, this approach will be the same improvement for IDT based technology for the 5GHz frequency range that IHP SAW was for the 2 GHz frequency range. Further inventions are expected based on ion-sliced LN layers in combination with other materials. Mm-wave acoustics is just at its incipit. Device demonstrations above 10 GHz have shown that microscale acoustic devices can outperform electromagnetic solutions at a significant fraction of the volume and weight. Curiosity in understanding material losses at microwave frequencies will drive fundamental research in this area and foster the discovery and invention of innovative acoustic resonator geometries best suited for operation at mm-waves. We expect that emerging applications in phased array communications will further motivate research activities and stimulate active development and deployment of exciting new mm-wave acoustic resonator technology.

ACKNOWLEDGMENT

The author Victor Plessky thanks J. Koskela and L.G. Villanueva and his colleagues from Resonant Inc. for support and numerous discussions and S. Yandrapalli for help.

REFERENCES

- [1] R. M. White and F. W. Voltmer, "Direct piezoelectric coupling to surface elastic waves," *Appl. Phys. Lett.*, vol. 7, no. 12, pp. 314–316, 1965.
- [2] Wikipedia, "Motorola dynatac," 2022. [Online]. Available: https://en.wikipedia.org/w/index.php?title=Motorola_DynaTAC&oldid=1109333356
- [3] YouTube, "Eevblog #243 - Vintage 1993/1994 brick mobile phone teardown," Feb. 7, 2012. Accessed: Oct. 09, 2022. [Online]. Available: <https://www.youtube.com/watch?v=7L3L2J-ljFA>
- [4] O. Ikata, T. Miyashita, T. Matsuda, T. Nishihara, and Y. Satoh, "Development of low-loss band-pass filters using saw resonators for portable telephones," in *Proc. IEEE Ultrason. Symp.*, 1992, pp. 111–115.
- [5] M. Kadota et al., "SAW substrate with coupling factor and excellent temperature stability suitable for duplexer of PCS in US," in *Proc. IEEE Ultrason. Symp.*, 2004, pp. 1970–1975.
- [6] J. Tsutsumi et al., "A miniaturized 3 × 3-mm SAW antenna duplexer for the US-PCS band with temperature-compensated LiTaO₃/sapphire substrate," in *Proc. IEEE Ultrason. Symp.*, 2004, pp. 954–958.
- [7] A. Hagelauer, G. Fattinger, C. C. W. Ruppel, M. Ueda, K.-Y. Hashimoto, and A. Tag, "Microwave acoustic wave devices: Recent advances on architectures, modeling, materials, and packaging," *IEEE Trans. Microw. Theory Techn.*, vol. 66, no. 10, pp. 4548–4562, Oct. 2018.
- [8] T. Takai et al., "Incredible high performance SAW resonator on novel multi-layered substrate," in *Proc. IEEE Int. Ultrason. Symp.*, 2016, pp. 1–4.
- [9] T. W. Grudkowski, J. F. Black, T. M. Reeder, D. E. Cullen, and R. A. Wagner, "Fundamental-mode VHF/UHF miniature acoustic resonators and filters on silicon," *Appl. Phys. Lett.*, vol. 37, no. 11, pp. 993–995, 1980.
- [10] K. Nakamura, H. Sasaki, and H. Shimizu, "A piezoelectric composite resonator consisting of a ZnO film on an anisotropically etched silicon substrate," *Jpn. J. Appl. Phys.*, vol. 20, no. S3, 1981, Art. no. 111.
- [11] K. M. Lakin, J. S. Wang, G. R. Kline, A. R. Landin, Y. Y. Chen, and J. D. Hunt, "Thin film resonators and filters," in *Proc. IEEE Ultrason. Symp.*, 1982, pp. 466–475.
- [12] J. S. Wang and K. M. Lakin, "Sputtered ALN films for bulk-acoustic-wave devices," in *Proc. IEEE Ultrason. Symp.*, 1981, pp. 502–505.
- [13] R. Ruby, Ed., *FBAR Filters and Resonators*. Norwood, MA, USA: Artech House, 2009.
- [14] M. Akiyama, T. Kamohara, K. Kano, A. Teshigahara, Y. Takeuchi, and N. Kawahara, "Enhancement of piezoelectric response in scandium aluminum nitride alloy thin films prepared by dual reactive cosputtering," *Adv. Mater.*, vol. 21, no. 5, pp. 593–596, 2009.
- [15] A. Tag et al., "Next generation of BAW: The new benchmark for RF acoustic technologies," in *Proc. IEEE Int. Ultrason. Symp.*, 2022, pp. 1–4, doi: [10.1109/IUS54386.2022.9958625](https://doi.org/10.1109/IUS54386.2022.9958625).
- [16] M. Gorisse et al., "Oriented single-crystal LiTaO₃ thin film on silicon for high performances SAW components," in *Proc. IEEE Int. Ultrason. Symp.*, 2018, pp. 1–4.
- [17] T. Takai et al., "I.H.P. saw technology and its application to micro-acoustic components (invited)," in *Proc. IEEE Int. Ultrason. Symp.*, 2017, pp. 1–8.
- [18] J. Hayashi et al., "High-coupling leaky SAWs on LiTaO₃ thin plate bonded to quartz substrate," in *Proc. IEEE Int. Ultrason. Symp.*, 2017, pp. 1–4.
- [19] M. Kadota and S. Tanaka, "Improved quality factor of hetero acoustic layer (HAL) SAW resonator combining LiTaO₃ thin plate and quartz substrate," in *Proc. IEEE Int. Ultrason. Symp.*, 2017, pp. 1–4.
- [20] S. Inoue and M. Solal, "Spurious free SAW resonators on layered substrate with ultra-high Q, high coupling and small TCF," in *Proc. IEEE Int. Ultrason. Symp.*, 2018, pp. 1–9.
- [21] S. Zhang et al., "Surface acoustic wave devices using lithium niobate on silicon carbide," *IEEE Trans. Microw. Theory Techn.*, vol. 68, no. 9, pp. 3653–3666, Sep. 2020.
- [22] S. Inoue, M. Solal, and R. Aigner, "SAW resonators with ultra-high Q high coupling and small TCF," in *Proc. IEEE Int. Symp. Acoust. Wave Devices Future Mobile Commun. Syst.*, 2018, pp. 1–9.
- [23] O. Kawachi, G. Endoh, M. Ueda, O. Ikata, E. Hashimoto, and M. Yamaguchi, "Optimum cut of LiTaO₃ for high performance leaky surface acoustic wave filters," in *Proc. IEEE Ultrason. Symp.*, 1996, pp. 71–76.
- [24] M. Solal, L. Chen, and J. Gratier, "Measurement and FEM/BEM simulation of transverse effects in SAW resonators in lithium tantalate," in *Proc. IEEE Int. Ultrason. Symp.*, 2010, pp. 175–180.
- [25] V. Plessky, "Transversely-excited film bulk acoustic resonator," U.S. Patent US10 491 192B1, Nov. 26, 2019.
- [26] V. Plessky, S. Yandrapalli, P. J. Turner, L. G. Villanueva, J. Koskela, and R. B. Hammond, "5 GHz laterally-excited bulk-wave resonators (XBARS) based on thin platelets of lithium niobate," *Electron. Lett.*, vol. 55, no. 2, pp. 98–100, 2019.
- [27] Jinan Jingzheng Electronics Co., Ltd. Accessed: May 22, 2018. [Online]. Available: <https://www.nanoln.com/PRODUCTS.html>

- [28] M. Kadota and T. Ogami, "5.4 GHz lamb wave resonator on LiNbO₃ thin crystal plate and its application," *Jpn. J. Appl. Phys.*, vol. 50, no. 7, 2011, Art. no. 07HD11.
- [29] S. Yandrapalli, S. E. K. Kucuk, B. Atakan, V. Plessky, and L. G. Villanueva, "Fabrication and analysis of thin film lithium niobate resonators for 5 GHz frequency and large Kt2 applications," in *Proc. IEEE Int. Conf. Micro Electro Mech. Syst.*, 2021, pp. 967–969.
- [30] S. Yandrapalli, S. E. K. Eroglu, V. Plessky, H. B. Atakan, and L. G. Villanueva, "Study of thin film LiNbO₃ laterally excited bulk acoustic resonators," *IEEE J. Microelectromech. Syst.*, vol. 31, no. 2, pp. 217–225, Apr. 2022.
- [31] V. Plessky, S. Küçük, S. Yandrapalli, and L. G. Villanueva, "A formula for the admittance of laterally excited bulk wave resonators (XBARs)," *Electron. Lett.*, vol. 57, no. 20, pp. 773–775, 2021.
- [32] P. J. Turner et al., "5 GHz band n79 wideband microacoustic filter using thin lithium niobate membrane," *Electron. Lett.*, vol. 55, no. 17, pp. 942–944, 2019.
- [33] J. Koulakis, J. Koskela, W. Yang, L. Myers, G. Dyer, and B. Garcia, "XBAR physics and next generation filter design," in *Proc. IEEE Int. Ultrason. Symp.*, 2021, pp. 1–5.
- [34] V. Plessky, "XBAR (invited)," in *Proc. IEEE Int. Ultrason. Symp.*, 2022, pp. 1–11.
- [35] K.-Y. Hashimoto, "Simulation of surface acoustic wave devices," *Jpn. J. Appl. Phys.*, vol. 45, no. 5B, pp. 4423–4428, 2006.
- [36] R. Lerch, "Simulation of piezoelectric devices by two- and three-dimensional finite elements," *IEEE Trans. Ultrason., Ferroelect., Freq. Control*, vol. 37, no. 3, pp. 233–247, May 1990.
- [37] R. K. Thalhammer and J. D. Larson, "Finite-element analysis of bulk-acoustic-wave devices: A review of model setup and applications," *IEEE Trans. Ultrason., Ferroelect., Freq. Control*, vol. 63, no. 10, pp. 1624–1635, Oct. 2016.
- [38] K.-Y. Hashimoto, Ed., *Coupling-of-Modes Theory*. Berlin, Germany: Springer-Verlag, 2000.
- [39] J. Koskela et al., "Hierarchical cascading in 2D FEM simulation of finite SAW devices with periodic block structure," in *Proc. IEEE Int. Ultrason. Symp.*, 2016, pp. 1–4.
- [40] J. Koskela, V. Plessky, B. Willemsen, P. Turner, B. Hammond, and N. Fenzi, "Hierarchical cascading algorithm for 2-D FEM simulation of finite SAW devices," *IEEE Trans. Ultrason., Ferroelect., Freq. Control*, vol. 65, no. 10, pp. 1933–1942, Oct. 2018.
- [41] K.-Y. Hashimoto, Y.-P. Wong, N. Matsuoka, X. Li, Y. Huang, and J. Bao, "Quantum leap in simulation technologies for radio frequency surface and bulk acoustic wave devices gifted by hierarchical cascading technique," in *Proc. IEEE Int. Ultrason. Symp.*, 2021, pp. 1–9.
- [42] J.-P. Berenger, "A perfectly matched layer for the absorption of electromagnetic waves," *J. Comput. Phys.*, vol. 114, no. 2, pp. 185–200, 1994.
- [43] X. Li, J. Bao, Y. Huang, B. Zhang, T. Omori, and K.-Y. Hashimoto, "Application of hierarchical cascading technique to finite element method simulation in bulk acoustic wave devices," *Jpn. J. Appl. Phys.*, vol. 57, no. 7S1, 2018, Art. no. 07LC08.
- [44] Y. Huang et al., "Analysis of SAW scattering with discontinuous periodic gratings using travelling wave excitation and hierarchical cascading technique," *IEEE Trans. Ultrason., Ferroelect., Freq. Control*, vol. 66, no. 7, pp. 1255–1263, Jul. 2019.
- [45] Y. He, T. Wu, Y.-P. Wong, T. B. Workie, J. Bao, and K.-Y. Hashimoto, "Impact of backward waves to FEM simulations of SAW resonators," in *Proc. IEEE Int. Conf. Microw. Acoust. Mech.*, 2022, pp. 74–77.
- [46] M. Solal, M. Gallagher, and A. Tajic, "Full 3D simulation of saw resonators using hierarchical cascading FEM," in *Proc. IEEE Int. Ultrason. Symp.*, 2017, pp. 1–5.
- [47] X. Li, J. Bao, L. Qiu, N. Matsuoka, T. Omori, and K.-Y. Hashimoto, "3D FEM simulation of SAW resonators using hierarchical cascading technique and general purpose graphic processing unit," *Jpn. J. Appl. Phys.*, vol. 58, no. SG, 2019, Art. no. SGGC05.
- [48] X. Li, J. Bao, Y. Huang, B. Zhang, T. Omori, and K.-Y. Hashimoto, "Use of hierarchical cascading technique for FEM analysis of transverse mode behaviors in surface acoustic wave devices," *IEEE Trans. Ultrason., Ferroelect., Freq. Control*, vol. 66, no. 12, pp. 1920–1926, Dec. 2019.
- [49] N. Matsuoka, X. Li, T. Omori, and K.-Y. Hashimoto, "Study of loss mechanisms in temperature compensated surface acoustic wave devices based on finite element method analysis using hierarchical cascading technique," *Jpn. J. Appl. Phys.*, vol. 59, no. SK, 2020, Art. no. SKKC06.
- [50] X. Li, J. Bao, Y. Huang, B. Zhang, T. Omori, and K.-Y. Hashimoto, "Traveling wave excitation sources for FEM analysis of scattering in acoustic waveguide," *Microsyst. Technol.*, vol. 25, no. 7, pp. 2783–2792, 2019.
- [51] F. Thalmayr, K.-Y. Hashimoto, T. Omori, and M. Yamaguchi, "Frequency domain analysis of lamb wave scattering and application to film bulk acoustic wave resonators," *IEEE Trans. Ultrason., Ferroelect., Freq. Control*, vol. 57, no. 7, pp. 1641–1648, Jul. 2010.
- [52] T. Wu, Y. He, Y. Wong, W. Li, J. Bao, and K. Hashimoto, "2D scalar wave modelling of apodized RF BAW resonators for transverse mode analysis," *Jpn. J. Appl. Phys.*, vol. 61, 2022, doi: 10.35848/1347-4065/aca5d8.
- [53] 3GPP, "Lte-advanced," Dec. 11, 2022. Accessed: Sep. 16, 2022. [Online]. Available: <https://www.3gpp.org/technologies/101-carrier-aggregation-explained>
- [54] B. A. Auld, *Acoustic Fields and Waves in Solids*, 2nd ed. Malabar, FL, USA: Krieger Publishing Company, 1990.
- [55] K.-Y. Hashimoto, *Surface Acoustic Wave Devices in Telecommunications: Modelling and Simulation*. Berlin, Germany: Springer, 2000.
- [56] G. Tobolka, "Mixed matrix representation of SAW transducers," *IEEE Trans. Sonics Ultrason.*, vol. 26, no. 6, pp. 426–427, Nov. 1979.
- [57] G. Kovacs, "A generalised p-matrix model for SAW filters," in *Proc. IEEE Symp. Ultrason.*, 2003, pp. 707–710.
- [58] R. Nakagawa, T. Suzuki, H. Shimizu, H. Kyoya, K. Nako, and K.-Y. Hashimoto, "Discussion about generation mechanisms of third-order nonlinear signals in surface acoustic wave resonators based on simulation," *Jpn. J. Appl. Phys.*, vol. 55, no. 7S1, 2016, Art. no. 07KD02.
- [59] S. Inoue et al., "A nonlinear elastic model for predicting triple beat in SAW duplexers," in *Proc. IEEE Int. Ultrason. Symp.*, 2011, pp. 1837–1841.
- [60] M. Mayer et al., "Rigorous com and p-matrix approaches to the simulation of third-order intermodulation distortion and triple beat in SAW filters," in *Proc. IEEE Int. Ultrason. Symp.*, 2013, pp. 1965–1968.
- [61] A. Mayer et al., "Full 2D-FEM calculations of third-order intermodulations in SAW devices," in *Proc. IEEE Int. Ultrason. Symp.*, 2016, pp. 1–4.
- [62] Y. Cho and K. Yamanouchi, "Nonlinear, elastic, piezoelectric, electrostrictive, and dielectric constants of lithium niobate," *J. Appl. Phys.*, vol. 61, no. 3, pp. 875–887, 1987.
- [63] H. Wang, "Theoretical strength of solids," Ph.D. dissertation, Georgia Inst. Technol., Atlanta, GA, USA, 2010. [Online]. Available: <https://smartech.gatech.edu/handle/1853/42747>
- [64] E. H. Bogardus, "Third-order elastic constants of Ge, MgO, and fused SiO₂," *J. Appl. Phys.*, vol. 36, no. 8, pp. 2504–2513, 1965.
- [65] K.-i. Kondo, S. Iio, and A. Sawaoka, "Nonlinear pressure dependence of the elastic moduli of fused quartz up to 3 GPa," *J. Appl. Phys.*, vol. 52, no. 4, pp. 2826–2831, 1981.
- [66] T. Forster et al., "Finite element simulations for predicting nonlinear responses of layered SAW systems," in *Proc. IEEE Int. Ultrason. Symp.*, 2021, pp. 1–4.
- [67] A. Tag et al., "A method for accurate modeling of baw filters at high power levels," *IEEE Trans. Ultrason., Ferroelect., Freq. Control*, vol. 63, no. 12, pp. 2207–2214, Dec. 2016.
- [68] V. Chauhan, A. Tag, M. Mayer, M. Pitschi, R. Weigel, and A. Hagelauer, "Modeling nonlinear behavior of RF bulk acoustic wave resonators," in *Proc. IEEE Int. Ultrason. Symp.*, 2016, pp. 1–4.
- [69] D. S. Shim and D. A. Feld, "A general nonlinear mason model of arbitrary nonlinearities in a piezoelectric film," in *Proc. IEEE Int. Ultrason. Symp.*, 2010, pp. 295–300.
- [70] Z. Cao, R. Liu, J. Wu, P.-L. Yu, and D. A. Feld, "Prediction of the H2 response of an FBAR resonator using finite element method," in *Proc. IEEE Int. Ultrason. Symp.*, 2018, pp. 1–5.
- [71] K.-Y. Hashimoto, X. Li, J. Bao, L. Qiu, and T. Omori, "Perturbation analysis of nonlinearity in radio-frequency bulk acoustic wave resonators using the mass-spring model," *IEEE Trans. Ultrason., Ferroelect., Freq. Control*, vol. 67, no. 7, pp. 1479–1484, Jul. 2020.
- [72] A. Tag et al., "Polyharmonic distortion modeling of RF BAW components," in *Proc. IEEE Int. Microw. Symp.*, 2015, pp. 1–4.
- [73] W. Akstaller, A. Tag, C. Musolf, R. Weigel, and A. Hagelauer, "Measurement setup for x-parameter characterization of bulk acoustic wave resonators," in *Proc. Microw. Meas. Conf.*, 2015, pp. 1–3.
- [74] A. Gimenez, J. Verdu, and P. de Paco Sanchez, "General synthesis methodology for the design of acoustic wave ladder filters and duplexers," *IEEE Access*, vol. 6, pp. 47969–47979, 2018.

- [75] S. Amari and G. Macchiarella, "Synthesis of inline filters with arbitrarily placed attenuation poles by using nonresonating nodes," *IEEE Trans. Microw. Theory Techn.*, vol. 53, no. 10, pp. 3075–3081, Oct. 2005.
- [76] A. Triano, J. Verdu, P. de Paco, T. Bauer, and K. Wagner, "Relation between electromagnetic coupling effects and network synthesis for AW ladder type filters," in *Proc. IEEE Int. Ultrason. Symp.*, 2017, pp. 1–4.
- [77] E. Guerrero, J. Verdu, and P. de Paco, "On the influence of input phase on the allocation of transmission zeros in acoustic ladder filters," in *Proc. IEEE Int. Microw. Filter Workshop*, 2021, pp. 102–105.
- [78] E. Guerrero, J. Verdu, and P. de Paco, "Synthesis of extracted pole filters with transmission zeros in both stopbands and nonresonant nodes of the same nature," *IEEE Microw. Wireless Compon. Lett.*, vol. 31, no. 1, pp. 17–20, Jan. 2021.
- [79] J. Verdu, P. de Paco, and Ó. Menendez, "Double-ladder filter topology for a dual-band transmission response based on bulk acoustic wave resonators," *IEEE Microw. Wireless Compon. Lett.*, vol. 20, no. 3, pp. 151–153, Mar. 2010.
- [80] J. Verdu, E. Guerrero, L. Acosta, and P. de Paco, "Exact synthesis of inline fully canonical dual-band filters using dual extracted-pole sections," *IEEE Microw. Wireless Compon. Lett.*, vol. 31, no. 12, pp. 1255–1258, Dec. 2021.
- [81] L. Acosta, E. Guerrero, J. Verdu, and P. de Paco, "Synthesis guidelines for acoustic wave standalone ladder filters with dual-band responses," in *Proc. IEEE Int. Microw. Symp.*, 2022, pp. 5–7.
- [82] E. Guerrero, L. Acosta, J. Verdu, and P. de Paco, "Analytical synthesis of acoustic wave duplexers and multiplexers," in *Proc. IEEE Int. Conf. Microw. Acoust. Mech.*, 2022, pp. 5–8.
- [83] L. Acosta, E. Guerrero, C. Caballero, J. Verdu, and P. de Paco, "Synthesis of acoustic wave multiport functions by using coupling matrix methodologies," in *Proc. IEEE Int. Conf. Microw. Acoust. Mech.*, 2022, pp. 56–59.
- [84] R. Ruby, "A snapshot in time: The future in filters for cell phones," *IEEE Microw. Mag.*, vol. 16, no. 7, pp. 46–59, Aug. 2015.
- [85] A. Konno, H. Hirano, M. Inaba, K.-Y. Hashimoto, M. Esashi, and S. Tanaka, "Tunable surface acoustic wave filter using integrated micro-electro-mechanical-system based varactors made of electroplated gold," *Jpn. J. Appl. Phys.*, vol. 52, no. 7S, 2013, Art. no. 07HD13.
- [86] K.-Y. Hashimoto et al., "Moving tunable filters forward: A heterointegration research project for tunable filters combining mems and RF SAW/BAW technologies," *IEEE Microw. Mag.*, vol. 16, no. 7, pp. 89–97, Aug. 2015.
- [87] A. Fouladi Azarnaminy and R. R. Mansour, "Switched dual-band SAW filters using hybrid and monolithically integrated vanadium oxide switches," *IEEE Trans. Microw. Theory Techn.*, vol. 70, no. 1, pp. 876–885, Jan. 2022.
- [88] G. Hummel, Y. Hui, and M. Rinaldi, "Reconfigurable piezoelectric MEMS resonator using phase change material programmable vias," *J. Microelectromech. Syst.*, vol. 24, no. 6, pp. 2145–2151, Dec. 2015.
- [89] T. H. Liu, X. Han, J. Pastrana, N. Sepúlveda, and J. Wang, "Piezoelectric lateral-extensional mode resonators with reconfigurable electrode and resonance mode-switching behavior enabled by a VO₂ thin-film," *IEEE Trans. Ultrason., Ferroelect., Freq. Control*, vol. 69, no. 8, pp. 2512–2525, Aug. 2022.
- [90] A. F. Azarnaminy, A. O. Suleiman, M. Chaker, and R. R. Mansour, "A reconfigurable SAW resonator using monolithically integrated switches," in *Proc. IEEE/MTT-S Int. Microw. Symp.*, 2022, pp. 806–808.
- [91] X. Zhu, J. D. Phillips, and A. Mortazawi, "A DC voltage dependant switchable thin film bulk wave acoustic resonator using ferroelectric thin film," in *Proc. IEEE Int. Microw. Symp.*, 2007, pp. 671–674.
- [92] J. Berge, A. Vorobiev, W. Steichen, and S. Gevorgian, "Tunable solidly mounted thin film bulk acoustic resonators based on Ba_xSr_{1-x}TiO₃ films," *IEEE Microw. Wireless Compon. Lett.*, vol. 17, no. 9, pp. 655–657, Sep. 2007.
- [93] A. Noeth, T. Yamada, A. K. Tagantsev, and N. Setter, "Electrical tuning of DC bias induced acoustic resonances in paraelectric thin films," *J. Appl. Phys.*, vol. 104, no. 9, 2008, Art. no. 094102.
- [94] X. Zhu, V. Lee, J. Phillips, and A. Mortazawi, "An intrinsically switchable FBAR filter based on barium titanate thin films," *IEEE Microw. Wireless Compon. Lett.*, vol. 19, no. 6, pp. 359–361, Jun. 2009.
- [95] A. Vorobiev, S. Gevorgian, M. Löffler, and E. Olsson, "Correlations between microstructure and Q-factor of tunable thin film bulk acoustic wave resonators," *J. Appl. Phys.*, vol. 110, no. 5, 2011, Art. no. 054102.
- [96] A. Vorobiev, J. Berge, S. Gevorgian, M. Löffler, and E. Olsson, "Effect of interface roughness on acoustic loss in tunable thin film bulk acoustic wave resonators," *J. Appl. Phys.*, vol. 110, no. 2, 2011, Art. no. 024116.
- [97] S. Lee, V. Lee, S. A. Sis, and A. Mortazawi, "Large-signal performance and modeling of intrinsically switchable ferroelectric FBARs," *IEEE Trans. Microw. Theory Techn.*, vol. 61, no. 1, pp. 415–422, Jan. 2013.
- [98] S. A. Sis, S. Lee, V. Lee, A. K. Bayraktaroglu, J. D. Phillips, and A. Mortazawi, "Intrinsically switchable, high-Q ferroelectric-silicon composite film bulk acoustic resonators," *IEEE Trans. Ultrason., Ferroelect., Freq. Control*, vol. 61, no. 2, pp. 231–238, Feb. 2014.
- [99] S. A. Sis, "Ferroelectric-on-silicon switchable bulk acoustic wave resonators and filters for RF applications," Ph.D. dissertation, Univ. Michigan, Ann Arbor, MI, USA, 2014. [Online]. Available: <https://deepblue.lib.umich.edu/handle/2027.42/107289>
- [100] S. Lee and A. Mortazawi, "An intrinsically switchable ladder-type ferroelectric BST-on-Si composite FBAR filter," *IEEE Trans. Ultrason., Ferroelect., Freq. Control*, vol. 63, no. 3, pp. 456–462, Mar. 2016.
- [101] S. Lee, M. Z. Koohi, and A. Mortazawi, "Lateral-wave spurious-modes elimination in switchable ferroelectric BST-on-Si composite FBARs," in *Proc. IEEE Int. Microw. Symp.*, 2016, pp. 1–4.
- [102] M. Z. Koohi, S. Lee, and A. Mortazawi, "High qmkt2 intrinsically switchable BST thin film bulk acoustic resonators," in *Proc. IEEE Int. Microw. Symp.*, 2017, pp. 296–299.
- [103] V. Lee, S. A. Sis, J. D. Phillips, and A. Mortazawi, "Intrinsically switchable ferroelectric contour mode resonators," *IEEE Trans. Microw. Theory Techn.*, vol. 61, no. 8, pp. 2806–2813, Aug. 2013.
- [104] V. C. Lee, "Switchable and tunable ferroelectric devices for adaptive and reconfigurable RF circuits," Ph.D. dissertation, Univ. Michigan, Ann Arbor, MI, USA, 2014. [Online]. Available: <https://deepblue.lib.umich.edu/handle/2027.42/107304>
- [105] S. Nam, M. Z. Koohi, W. Peng, and A. Mortazawi, "A switchless quad band filter bank based on ferroelectric BST FBARs," *IEEE Microw. Wireless Compon. Lett.*, vol. 31, no. 6, pp. 662–665, Jun. 2021.
- [106] S. Gevorgian and A. Vorobiev, "Impedance of DC-bias-controlled composite FBARs," *IEEE Trans. Ultrason., Ferroelect., Freq. Control*, vol. 60, no. 4, pp. 795–804, Apr. 2013.
- [107] S. V. Ptashnik et al., "Ferroelectric thin film acoustic devices with electrical multiband switching ability," *Sci. Rep.*, vol. 7, no. 1, 2017, Art. no. 15289.
- [108] M. Z. Koohi and A. Mortazawi, "Switched mode thin film bulk acoustic wave resonators," in *Proc. IEEE Int. Microw. Symp.*, 2019, pp. 528–531.
- [109] S. Nam, D. Psychogiou, and A. Mortazawi, "Reconfigurable transfer function BST acoustic wave lumped element resonator filters," in *Proc. IEEE Eur. Microw. Conf.*, 2022, pp. 301–304.
- [110] M. Hara, T. Yokoyama, T. Sakashita, M. Ueda, and Y. Satoh, "A study of the thin film bulk acoustic resonator filters in several ten GHz band," in *Proc. IEEE Int. Ultrason. Symp.*, 2009, pp. 851–854.
- [111] M. Hara et al., "Super-high-frequency band filters configured with air-gap-type thin-film bulk acoustic resonators," *Jpn. J. Appl. Phys.*, vol. 49, no. 7, 2010, Art. no. 07HD13.
- [112] M. Rinaldi, C. Zuniga, and G. Piazza, "5–10 GHz AIN contour-mode nanoelectromechanical resonators," in *Proc. IEEE Int. Conf. Micro Electro Mech. Syst.*, 2009, pp. 916–919.
- [113] M. Park, Z. Hao, D. G. Kim, A. Clark, R. Dargis, and A. Ansari, "A 10 GHz single-crystalline scandium-doped aluminum nitride lamb-wave resonator," in *Proc. IEEE Int. Conf. Solid-State Sensors, Actuators Microsyst. Eurosensors XXXIII*, 2019, pp. 450–453.
- [114] G. Giribaldi et al., "X-band multi-frequency 30% compound SCALN microacoustic resonators and filters for 5G-advanced and 6G applications," in *Proc. IEEE Joint Conf. Eur. Freq. Time Forum IEEE Int. Freq. Control Symp.*, 2022, pp. 1–4.
- [115] M. Assylbekova, G. Chen, M. Pirro, G. Michetti, and M. Rinaldi, "Aluminum nitride combined overtone resonator for millimeter wave 5G applications," in *Proc. IEEE Int. Conf. Micro Electro Mech. Syst.*, 2021, pp. 202–205.
- [116] G. Chen and M. Rinaldi, "Aluminum nitride combined overtone resonators for the 5G high frequency bands," *IEEE J. Microelectromech. Syst.*, vol. 29, no. 2, pp. 148–159, Apr. 2020.

- [117] D. Mo, S. Dabas, S. Rassay, and R. Tabrizian, "Complementary-switchable dual-mode SHF scandium aluminum nitride BAW resonator," *IEEE Trans. Electron Devices*, vol. 69, no. 8, pp. 4624–4631, Aug. 2022. [Online]. Available: <https://arxiv.org/pdf/2205.03446>
- [118] B. Bahr, Y. He, Z. Krivokapic, S. Banna, and D. Weinstein, "32 GHz resonant-fin transistors in 14 nm FinFET technology," in *Proc. IEEE Int. Solid-State Circuits Conf.*, 2018, pp. 348–350.
- [119] M. Ghatge, G. Walters, T. Nishida, and R. Tabrizian, "High-Q UHF and SHF bulk acoustic wave resonators with ten-nanometer Hf_{0.5}Zr_{0.5}O₂ ferroelectric transducer," in *Proc. IEEE Int. Conf. Solid-State Sensors, Actuators Microsyst. Eurosensors XXXIII*, 2019, pp. 446–449.
- [120] F. Hakim, T. Tharpe, and R. Tabrizian, "Ferroelectric-on-Si super-high-frequency fin bulk acoustic resonators with Hf_{0.5}Zr_{0.5}O₂ nanolaminated transducers," *IEEE Microw. Wireless Compon. Lett.*, vol. 31, no. 6, pp. 701–704, Jun. 2021.
- [121] Y. Yang, R. Lu, T. Manzanique, and S. Gong, "Toward Ka band acoustics: Lithium niobate asymmetrical mode piezoelectric mems resonators," in *Proc. IEEE Int. Freq. Control Symp.*, 2018, pp. 1–5.
- [122] R. Lu and S. Gong, "A 15.8 GHz A6 mode resonator with Q of 720 in complementarily oriented piezoelectric lithium niobate thin films," in *Proc. IEEE Joint Conf. Eur. Freq. Time Forum/IEEE Int. Freq. Control Symp.*, 2021, pp. 1–4.
- [123] S. Gong, R. Lu, Y. Yang, L. Gao, and A. E. Hassanien, "Microwave acoustic devices: Recent advances and outlook," *IEEE J. Microwaves*, vol. 1, no. 2, pp. 601–609, Apr. 2021.
- [124] Y. Yang, R. Lu, L. Gao, and S. Gong, "10–60-GHz electromechanical resonators using thin-film lithium niobate," *IEEE Trans. Microw. Theory Techn.*, vol. 68, no. 12, pp. 5211–5220, Dec. 2020.
- [125] Y. Yang, L. Gao, and S. Gong, "X-band miniature filters using lithium niobate acoustic resonators and bandwidth widening technique," *IEEE Trans. Microw. Theory Techn.*, vol. 69, no. 3, pp. 1602–1610, Mar. 2021.
- [126] Z. Schaffer, P. Simeoni, and G. Piazza, "33 GHz overmoded bulk acoustic resonator," *IEEE Microw. Wireless Compon. Lett.*, vol. 32, no. 6, pp. 656–659, Jun. 2022.
- [127] D. S. Yu et al., "Narrow-band band-pass filters on silicon substrates at 30 GHz," in *Proc. IEEE Int. Ultrason. Symp.*, 2004, pp. 1467–1470.
- [128] G. W. Pierce, "Piezoelectric crystal resonators and crystal oscillators applied to the precision calibration of wavemeters," *Proc. Amer. Acad. Arts Sci.*, vol. 59, no. 4, pp. 81–106, 1923.
- [129] E. T.-T. Yen et al., "Integrated high-frequency reference clock systems utilizing mirror-encapsulated BAW resonators," in *Proc. Int. Ultrason. Symp.*, 2019, pp. 2174–2177.
- [130] A. Partridge, A. E. Rice, T. W. Kenny, and M. Lutz, "New thin film epitaxial polysilicon encapsulation for piezoresistive accelerometers," in *Proc. IEEE Int. Conf. Micro Electro Mech. Syst.*, 2001, pp. 54–59.
- [131] W.-t. Hsu, "Vibrating RF mems for timing and frequency references," in *Proc. IEEE Int. Microw. Symp.*, 2006, pp. 672–675.
- [132] A. Franke, R. Howe, and T.-J. King, "Polycrystalline silicon-germanium films for micro-electromechanical systems application," U.S. Patent US-6448622-B1, Grant 2002/09/10. [Online]. Available: <https://pubchem.ncbi.nlm.nih.gov/patent/US-6448622-B1>
- [133] A. Jaakkola, P. Pekko, J. Dekker, M. Prunnila, and T. Pensala, "Second order temperature compensated piezoelectrically driven 23 MHz heavily doped silicon resonators with PPM temperature stability," in *Proc. Joint Conf. IEEE Int. Freq. Control Symp. Eur. Freq. Time Forum*, 2015, pp. 420–422.
- [134] V. Kaajakari et al., "A 32.768 kHz MEMS resonator with +/-20 ppm tolerance in 0.9 mm x 0.6 mm chip scale package," in *Proc. Joint Conf. IEEE Int. Freq. Control Symp. Eur. Freq. Time Forum*, 2019, pp. 1–4.
- [135] J. H. Kuypers, "High frequency oscillators for mobile devices," in *Piezoelectric MEMS Resonators* (Microsystems and Nanosystems Series), H. Bhugra and G. Piazza, Eds. Cham, Switzerland: Springer, 2017, pp. 335–385.
- [136] E. A. Vittoz, "The design of low-power high-Q oscillators," in *MEMS-based Circuits and Systems for Wireless Communication*, C. C. Enz and A. Kaiser, Eds. Boston, MA, USA: Springer US, 2013, pp. 121–154.
- [137] A. Khanna, E. Gane, and T. Chong, "A 2 GHz voltage tunable FBAR oscillator," in *Proc. IEEE Int. Microw. Symp.*, 2003, pp. 717–720.
- [138] S. S. Rai and B. P. Otis, "A 600 UW BAW-tuned quadrature VCO using source degenerated coupling," *IEEE J. Solid-State Circuits*, vol. 43, no. 1, pp. 300–305, Jan. 2008.
- [139] M. Aissi, E. Tourmier, M. A. Dubois, C. Billard, H. Ziad, and R. Plana, "A 5 GHz above-IC FBAR low phase noise balanced oscillator," in *Proc. IEEE Radio Freq. Integr. Circuits Symp.*, 2006, pp. 25–28.
- [140] D. Griffith et al., "3.1 an integrated baw oscillator with ± 30 ppm frequency stability over temperature, package stress, and aging suitable for high-volume production," in *Proc. IEEE Int. Solid State Circuits Conf.*, 2020, pp. 58–60.
- [141] S. Mukherjee et al., "A 0.5-to-400MHz programmable BAW oscillator with fractional output divider achieving 4 PPM frequency stability over temperature and <math>< 95</math>fs jitter," in *Proc. IEEE Int. Solid State Circuits Conf.*, 2023, early access.
- [142] R. Wojtyna, "Long-term and short-term frequency stabilities in sinusoidal oscillators," in *Proc. IEEE Int. Symp. Circuits Syst.*, 1988, pp. 639–641.
- [143] E. J. Ng, V. A. Hong, Y. Yang, C. H. Ahn, C. L. M. Everhart, and T. W. Kenny, "Temperature dependence of the elastic constants of doped silicon," *IEEE J. Microelectromech. Syst.*, vol. 24, no. 3, pp. 730–741, Jun. 2015.
- [144] A. Jaakkola, M. Prunnila, T. Pensala, J. Dekker, and P. Pekko, "Determination of doping and temperature-dependent elastic constants of degenerately doped silicon from MEMS resonators," *IEEE Trans. Ultrason., Ferroelect., Freq. Control*, vol. 61, no. 7, pp. 1063–1074, Jul. 2014.
- [145] R. Ruby, "Ultra-small high frequency zero drift resonators and oscillators for non-gps quartz crystal applications," in *Proc. IEEE 8th Int. NEWCAS Conf.*, 2010, pp. 157–160.
- [146] *IEEE Standard for Low-Rate Wireless Networks*, IEEE Standard 802.15.4-2020 (Revision of IEEE Std 802.15.4-2015), 2020.
- [147] ETSI Technical Specification 136 106, 2020.
- [148] Crystal Units, Quartz, General Specification for, MIL-PRF-3098K, 2014.
- [149] J. Segovia-Fernandez, Y. Suzuki, M. Chowdhury, J. Rojas, and E. T.-T. Yen, "A thermal-stress FEM to predict aging in packaged mems resonators," in *Proc. IEEE Joint Conf. Eur. Freq. Time Forum/IEEE Int. Freq. Control Symp.*, 2022, pp. 1–3.
- [150] S. Sridaran et al., "Low jitter FBAR based chip scale precision oscillator," in *Proc. IEEE Int. Ultrason. Symp.*, 2014, pp. 85–88.
- [151] J. Segovia-Fernandez, E. Tuncer, S. Chang, and E. T.-T. Yen, "Time-temperature superposition based accelerated aging method for packaged MEMS resonators," in *Proc. IEEE Joint Conf. Eur. Freq. Time Forum/IEEE Int. Freq. Control Symp.*, 2022, pp. 1–4.
- [152] E. T.-T. Yen, B. Kramer, T. Tarsi, D. Griffith, and B. Goodlin, "A multi-tone testing technique for production characterization of micro-resonators," in *Proc. IEEE 30th Int. Conf. Micro Electro Mech. Syst.*, 2017, pp. 80–83.



AMELIE HAGELAUER (Senior Member, IEEE) received the Dipl.-Ing. degree in mechatronics and the Dr.-Ing. degree in electrical engineering from Friedrich-Alexander-University (FAU) Erlangen-Nuremberg, Erlangen, Germany, in 2007 and 2013, respectively, and the Ph.D. degree in bulk acoustic wave (BAW) resonators and filters from the Institute for Electronics Engineering, FAU. In November 2007, she joined the Institute for Electronics Engineering, FAU, for the Ph.D. degree. Since 2013, she has been focusing on surface acoustic wave (SAW)/BAW, RF microelectromechanical systems components, and microwave integrated circuits for frontends. From 2016 to 2019, she was leading a Research Group on Electronic Circuits and from August 2019 to September 2021, she was a Full Professor with the University of Bayreuth, Bayreuth, Germany. In September 2021, she joined the Technical University of Munich, Munich, Germany, as a Full Professor and became the Co-Director of the Fraunhofer EMFT Research Institution for Microsystems and Solid State Technologies, Munich. She has authored or coauthored more than 140 peer-reviewed publications in her research fields, which include research and development of microwave theory and technology, electronic circuits and systems, and communication and sensing systems.



RICH RUBY (Fellow, IEEE) started his work on FBARs with HP Labs, Palo Alto, CA, USA, in 1993. He introduced the first FBAR product for cell phone applications, the Dick Tracy Wristwatch Phone by Samsung, in 2000, and in the Sanyo “Slim Phone” in 2001. These products were the first commercially viable AlN deposition film technology with molybdenum electrodes that blended acoustics with MEMS. The excellent performance and ultra-small size of this new technology changed the course of filter technology that

then led the way to extremely small, ultra-high performance filters, duplexers and multiplexers and integrated filter/PA/LNA modules. In 2004, he introduced an all-silicon, packaged FBAR filter and since then, has made seminal contributions to the Q and coupling coefficient of FBAR. In 2007, he also began to branch out from filter applications, developing a GaAS cap package for the microwave division and several innovative stress-insensitive FBAR resonators for oscillators used in the time and frequency space and also ultra-low energy transmitter devices. In 2010, he started work on Sc-doped AlN (ASN) leading to the first commercial ASN product (in iPhones) introduced in 2016 and 2017. Today, BAW filters can be found in cellphones used around the world. He is currently spearheading development of silicon SAW products to round out the technology portfolio of Broadcom’s Wireless Business. He was the recipient of the Industrial Application of Physics Prize awarded by the American Institute of Physics, College Park, MD, USA, C.B. Sawyer Memorial Award, Bill Hewlett Award and the Barney Oliver Award, and most recently the Distinguished Alumni Award from the University of California Berkeley, Berkeley, CA, USA.



VICTOR PLESSKY (Senior Member, IEEE) was born in Gomel, Belarus, on 2 July 1952. He received the Ph.D. degree from Moscow Physical-Technical Institute, Dolgoprudny, Russia (“FizTech”) in 1978, and the D.Sc. degree from the Russian Government in 1987. He has worked more than 45 years in the area of surface acoustic wave physics and devices. He predicted theoretically (together with Yu. Gulyaev and independently from Auld, Gagnepain, and Tan) the existence of surface transverse waves, a new type of waves now used

for design of high- Q GHz frequency range resonators. His theory of the leaky wave propagation in periodic grating (so-called “Plessky equation”) was basic for understanding of the leaky waves propagation characteristics. Recently, he invented XBARS—Thin lithium niobate film resonators operating as laterally excited A1 Lamb mode. He has authored or coauthored more than 300 papers and holds about 50 patents. His current research interests include area of micro/nano acoustic physics and devices. As a Visiting Professor, he collaborated many years with the Helsinki University of Technology, Espoo, Finland. He was lecturing with Freiburg University, Ecole Polytechnique Fralre de Lausanne, Lausanne, Switzerland, and Angstrom Lab, Uppsala, Sweden. He also held position of Chair of Excellence in ENSMM (Technical University, Institute FEMTO) in Besançon, France, during 2011–2012. He was supervisor and consultant of 15 Ph.D. dissertations. Dr. Plessky holds a title of “Full Professor” granted to him by the Russian Government in 1995. He was the recipient of the Lenin Komsomol Award (3rd state Premium in ex-USSR) for young scientists, 1978, and Outstanding Paper Award from IEEE in 2001. He was the recipient of Sawyer Award from IEEE Frequency Control Symposium in 2019. He served for many years in TPCs of IEEE IUS, and other conferences. Currently, he is retired but continues to work as a consultant and lecturer.



KEN-YA HASHIMOTO (Life Fellow, IEEE) was born in Fukushima, Japan, in 1956. He received the B.S. and M.S. degrees in electrical engineering from Chiba University, Chiba, Japan, in 1978 and 1980, respectively, and the D.Eng. degree from Tokyo Institute of Technology, Tokyo, Japan, in 1989. He joined Chiba University, as a Research Associate in 1980 and retired as a Professor Emeritus in 2021. From 2013 to 2015, he was the Director of the Center for the Frontier Science with Chiba University. After the retirement, he moved

to the University of Electronic Science and Technology of China (UESTC), Chengdu, China, as a Professor. He had Visiting Professor/Researcher positions in various institutions, such as the Helsinki University of Technology, Espoo, Finland, in 1998; Laboratoire de Physique et Metrologie des Oscillateurs, CNRS, Besançon, France, from 1998 to 1999; Johannes Kepler University, Linz, Austria, from 1999 to 2001; Institute of Acoustics, Chinese Academy of Science, Beijing, China, from 2005 to 2006; UESTC from 2009 to 2012; and Shanghai Jiao Tong University, Shanghai, China, in 2015. His research interests include simulation and design of various high-performance surface and bulk acoustic wave devices, acoustic wave sensors and actuators, piezoelectric materials, and RF circuit design. He was a Guest Co-Editor of the IEEE TRANSACTIONS ON MICROWAVE THEORY AND TECHNIQUES Special Issue on Microwave Acoustic Wave Devices for Wireless Communications in 2001, and Publicity Co-Chair of the 2002, 2015, and 2021 IEEE International Ultrasonics Symposia, an International Distinguished Lecturer of the IEEE Ultrasonics, Ferroelectrics, and Frequency Control Society from 2005 to 2006, Administrative Committee Member of the IEEE UFFC Society from 2007 to 2009 and from 2014 to 2016, a Distinguished Lecturer of the IEEE Electron Devices Society from 2007 to 2009, and General Co-Chair of the 2011 and 2018 IEEE International Ultrasonics Symposia. He was the recipient of the Ichimura Industrial Award from the New Technology Development Foundation for Development of Optimal Substrate 42-LT for Radio Frequency Surface Acoustic Wave Devices in 2015, Commendation for Science and Technology by the Minister of Education, Culture, Sports, Science and Technology for Research on High Performance Radio Frequency Surface Acoustic Wave Devices in 2018, and Distinguished Service Award from the IEEE UFFC Society in 2019.



SHOGO INOUE (Member, IEEE) received the B.S., M.S., and Ph.D. degrees in electronic engineering from Osaka University, Osaka, Japan, in 1998, 2000, and 2008, respectively. His Doctoral dissertation is titled “A Study on Design Techniques for High Performance RF SAW Filters/Duplexers.” From 2000 to 2013, he was with Fujitsu Laboratories Ltd., Akashi, Japan, which became Taiyo Yuden Company, Ltd., in 2010. From 2009 to 2010, he was a Visiting Scholar with the Berkeley Sensor and Actuator Center, University

of California, Berkeley, CA, USA. In 2013, he joined Triquint Semiconductor, Inc., Apopka, FL, USA. He holds more than 70 U.S. patents and has authored or coauthored more than 40 papers, including one technical book on SAW devices. Dr. Inoue is currently a Fellow of Acoustic Technology R&D, Qorvo, Inc., Apopka, and involved in research and development of innovative RF microacoustic technologies. Since 2017, he has been a Technical Program Committee Member of the IEEE International Ultrasonics Symposium, Group 4: Microacoustics – SAW, BAW, and MEMS. He was the recipient of the Electronics Society Excellent Letter Award from the Institute of Electronics, Information and Communication Engineers, Tokyo, Japan, in 2008.



RYO NAKAGAWA (Member, IEEE) was born in Shiga Prefecture, Japan, in 1978. He received the B.S. and M.S. degrees in electrical engineering, and the Ph.D. degree from Chiba University, Chiba, China, in 2001, 2003, and 2016, respectively. His master's thesis and doctoral dissertation concerned an Analysis Technique of Transverse Modes of SAW Devices and Generation Mechanisms of Nonlinearity in SAW Devices, respectively. He joined Murata Manufacturing Company, Ltd., Japan, in 2003. His research interests include

development of SAW filters and duplexers. He is currently a Principal Researcher of the SAW technology Development Department. Since 2016, Dr. Nakagawa has been a member of Technical Program Committee of the IEEE International Ultrasonic Symposium.



JORDI VERDU (Senior Member, IEEE) was born in Sabadell, Spain. He received the M.S. degree in telecommunication engineering and the Ph.D. degree (*cum laude*) from the Universitat Autònoma de Barcelona, Bellaterra, Spain, in 2006 and 2010, respectively. From 2006 to 2010, he was a Member of Antenna and Microwave Systems. In 2010, he joined the RF System Group, European Spallation Source in Bilbao (ESS-B), where he was the Group Coordinator. During 2011–2012, he was with the École Polytechnique Fédérale de Lausanne, Lau-

sanne, Switzerland, through a Marie Curie grant. In 2013, he joined the Theory Signal Communication Group, Universitat Politècnica de Catalunya, Barcelona, Spain. He is currently an Associate Professor with the Universitat Autònoma de Barcelona, where he teaches microwave engineering courses. He is a member of the MTT-6 MEMS and Microwave Acoustics Technical Committee, and reviewer of several transactions and letters of the IEEE. He has participated in several national and international projects mostly related to the design of acoustic wave filters. His research interests include the design of microwave devices, linear modeling, and the design of active devices for space applications. He was the recipient of the Department Best Thesis Prize.



PEDRO DE PACO (Senior Member, IEEE) was born in Badalona, Spain. He received the M.S. degree in telecommunication engineering and the Ph.D. degree (*cum laude*) from the Universitat Politècnica de Catalunya (UPC), Barcelona, Spain, in 1997 and 2003, respectively. In 1998, he joined the Electromagnetic and Photonics Engineering Group, Signal Theory and Communications Department (TSC-UPC) with a grant from the Institut d'Estudis Espacials de Catalunya, Barcelona, Spain, in a joint activity related with the European

Scientific Space Mission Planck. He was a member of the LFI-Radiometer working group and the Planck Consortium. During his Ph.D., and UPC stage participated in several national and international research projects mostly related to microwave and millimeter-wave circuits and systems applied to design and testing of remote sensing instruments and front-end point-to-multipoint broad-band communication system. Since 2004, he has been an Associate Professor with the Universitat Autònoma de Barcelona, Bellaterra, Spain, where he teaches applied electromagnetics and microwave engineering courses. He has advised eight Ph.D. students. From 2010 to 2013, he was the Deputy Director and Member of the Executive Board in the Telecommunication and System Engineering Department, University of Alabama at Birmingham, Birmingham, AL, USA. During 2018–2019, he was a Visiting Researcher with the Microwave and RF Research Group, Colorado University-Boulder, Boulder, CO, USA. His research interests include microwave filter synthesis and microwave acoustics filter synthesis and design, and also microwave and radar systems and devices. He has been appointed as a Technical Expert for Telecommunications Equipment by the National Agency of Accreditation. He is a member of MTT-6 RF MEMS and Microwave Acoustics Committee, and a reviewer of IEEE TRANSACTIONS ON MICROWAVE THEORY AND TECHNIQUES and IEEE MICROWAVE AND WIRELESS COMPONENTS LETTERS. He is also a member of the Technical Review Board for the European Microwave Conference. He was awarded three times with merits in research and recognized with merits in University training by l'Agència de Qualitat, and awarded with Advanced Research by Generalitat Catalunya.



AMIR MORTAZAWI (Fellow, IEEE) received the Ph.D. degree in electrical engineering from The University of Texas at Austin, Austin, TX, USA, in 1990. He is currently a Professor of electrical engineering with the University of Michigan at Ann Arbor, Ann Arbor, MI, USA. His research interests include millimeter-wave phased arrays, power amplifiers, power-combining techniques, wireless power transmission and harvesting, and frequency-agile microwave circuits. Dr. Mortazawi was an

Elected Member of the IEEE MTT-S Administrative Committee (AdCom) for eight years. He was the recipient of the 2019 Distinguished Educator Award from the IEEE Microwave Theory and Techniques Society. He is also the Chair of the MTT-S Distinguished Microwave Lecturers Committee. From 2006 to 2010, he was the Editor-in-Chief of IEEE TRANSACTIONS ON MICROWAVE THEORY AND TECHNIQUES. He was an Associate Editor for IEEE TRANSACTIONS ON MICROWAVE THEORY AND TECHNIQUES in 2005 and IEEE TRANSACTIONS ON ANTENNAS AND PROPAGATION from 1998 to 2010, and the Guest Editor of the Special Issue on the IEEE MTT-S Microwave Symposium for IEEE TRANSACTIONS ON MICROWAVE THEORY AND TECHNIQUES in December 1995.



GIANLUCA PIAZZA (Senior Member, IEEE) is currently an ST Microelectronics Professor with the Department of Electrical and Computer Engineering, Carnegie Mellon University, Pittsburgh, PA, USA, and the Director of the CMU Nanofabrication Facility, Pittsburgh. His research interests include piezoelectric micro and nano electromechanical systems (M/NEMS) for RF wireless communication, acousto-optics, chemical/biological detection, ultrasonics, and mechanically-assisted computing. He also has a general interest in the

areas of micro/nano fabrication techniques and integration of micro/nano devices with state-of-the-art electronics. He has more than 20 years of experience working with piezoelectric materials and devices. He holds several patents in the field of micromechanical resonators some of which have been acquired by industry. He was the recipient of the IBM Young Faculty Award in 2006 and Best Paper Award at the IEEE Frequency Control Symposium in 2008, 2009, 2011 and 2013, at the IEEE Ultrasonic Symposium in 2012 and at the IEEE IMS 2022 with his students. He was the Editor-in-Chief of IEEE JOURNAL OF MICROELECTROMECHANICAL SYSTEMS.



ZACHARY SCHAFFER (Student Member, IEEE) received the bachelor's degree in nanoscale engineering from the State University of New York Polytechnic Institute, Albany, NY, USA, in 2017, and the Ph.D. degree from Carnegie Mellon University, Pittsburgh, PA, USA. His research interests include designing novel micro- and nanoelectromechanical systems for RF applications and investigating the materials that comprise them. He is currently working to develop practical mm-wave acoustic resonators through novel device design

and characterization of loss. He was the recipient of the Best Student Paper Award at IEEE IMS in 2022 and is a finalist at IEEE IUS 2022.



ERNEST TING-TA YEN (Member, IEEE) received the double B.S. degree in electrical engineering and power mechanical engineering from National Tsing Hua University, Hsinchu, Taiwan, in 2004, the M.S. degree in electrical engineering from the University of California, Berkeley, Berkeley, CA, USA, in 2012, and the Ph.D. degree in mechanical engineering from the University of California, Berkeley, in 2012. After his Ph.D. degree, he joined the Kilby Labs, Texas Instruments, Santa Clara, CA, USA, as a MEMS technologist. His research

interests include piezoelectric MEMS in RF and sensing applications. He developed the DBAR (dual-Bragg acoustic resonator) in TI, integrated it into several system chips, and commercialized it in 2018. He currently holds an SMTS (senior member, technical staff) title and leads the MEMS R&D Team along with several university research collaborations in the Kilby Labs, focusing on RF MEMS, nano-mechanical circuit, sensors, and advanced package. Dr. Yen is an active reviewer of top MEMS journals, including *Journal of Microelectromechanical Systems*, and *Sensors*. He is elected as the Vice-Chair of the IEEE SFBA (San Francisco Bay Area) MEMS and Sensor Chapter during 2016–2017. Besides his engineering carrier, he is also a concert Violinist toured with orchestras across North America, Europe, and Asia.



THOMAS FORSTER (Student Member, IEEE) was born in Schwandorf, Germany, in 1995. He received the B.Eng. degree in electrical engineering from the Technical University of Applied Sciences Amberg-Weiden, Amberg, Germany, in 2018, and the M.Eng. degree in electrical and microsystems engineering from the Technical University of Applied Sciences Regensburg, Regensburg, Germany, in 2019. Since 2020, he has been working toward the Ph.D. degree with the University of Bayreuth, Bayreuth, Germany, in cooperation with an industry partner. In October 2021, he transitioned to the Technical University of Munich, Munich, Germany, where he is currently working on his Ph.D. project. His research interests include micro acoustic filters for mobile communications, especially their nonlinear modeling. He was the recipient of the Student Best Paper Award at the IEEE International Ultrasonics Symposium 2021.



ANDREAS TAG (Member, IEEE) received the B.S.E.E. and M.S.E.E. degrees from the Technische Universität München, Munich, Germany, in 2010 and 2012, respectively, and the Doctor of Engineering degree in multi physical modeling and optimization of micro acoustic RF MEMS components from the Friedrich-Alexander Universität Erlangen-Nürnberg, Erlangen, Germany, in March 2016. In August 2015, he joined Qorvo Inc., Greensboro, NC, USA, as a member of Technical Staff, where he is currently driving the develop-

ment and release of new generations of RF acoustic wave technologies. His research interests include RF MEMS and Acoustics technologies, microwave measurement techniques and instruments, and electronic design automation. Dr. Tag was nominated for the best paper award at the European Microwave Conference 2013 and was the finalist of the student paper competition at the IEEE International Ultrasonic Symposium in 2014 and 2015, respectively. He was the recipient of several awards like the 2019 VDE-ITG (German Association for Electrical, Electronic and Information Technologies - Information Technology Society) Award, Qorvo's Core Award, and Qorvo's Best Technology Award 2022. He is continuously contributing to the development of RF Acoustics community by organizing workshops, student design competitions and by acting as a Guest Editor. Examples are workshops "RF Acoustics" and "Acoustic Multiplexer for Carrier Aggregation," and the yearly organization of the student design competitions "SAW triplexer" and "BAW Quadplexer Module" for the International Microwave Symposiums between 2015 and 2019. He has been acting as a Guest Editor of the special issue of *IEEE Microwave Magazine* on the topic RF acoustic for mobile communication - challenges and solutions and IEEE TRANSACTIONS ON MICROWAVE THEORY AND TECHNIQUES on the topic RF Frontends for Mobile Radio Terminal Applications. As the General Co-Chair he was also involved into launching a new IEEE MTT-S International Conference on Microwave Acoustics and Mechanics in 2022. He was acting as the Vice Chair of the MTT Microwave Acoustics Technical Committee and MTT RF MEMS and Microwave Acoustics Technical Committee and become the Chair in 2021. He is also a member of VDE (German Association for Electrical, Electronic and Information Technologies).